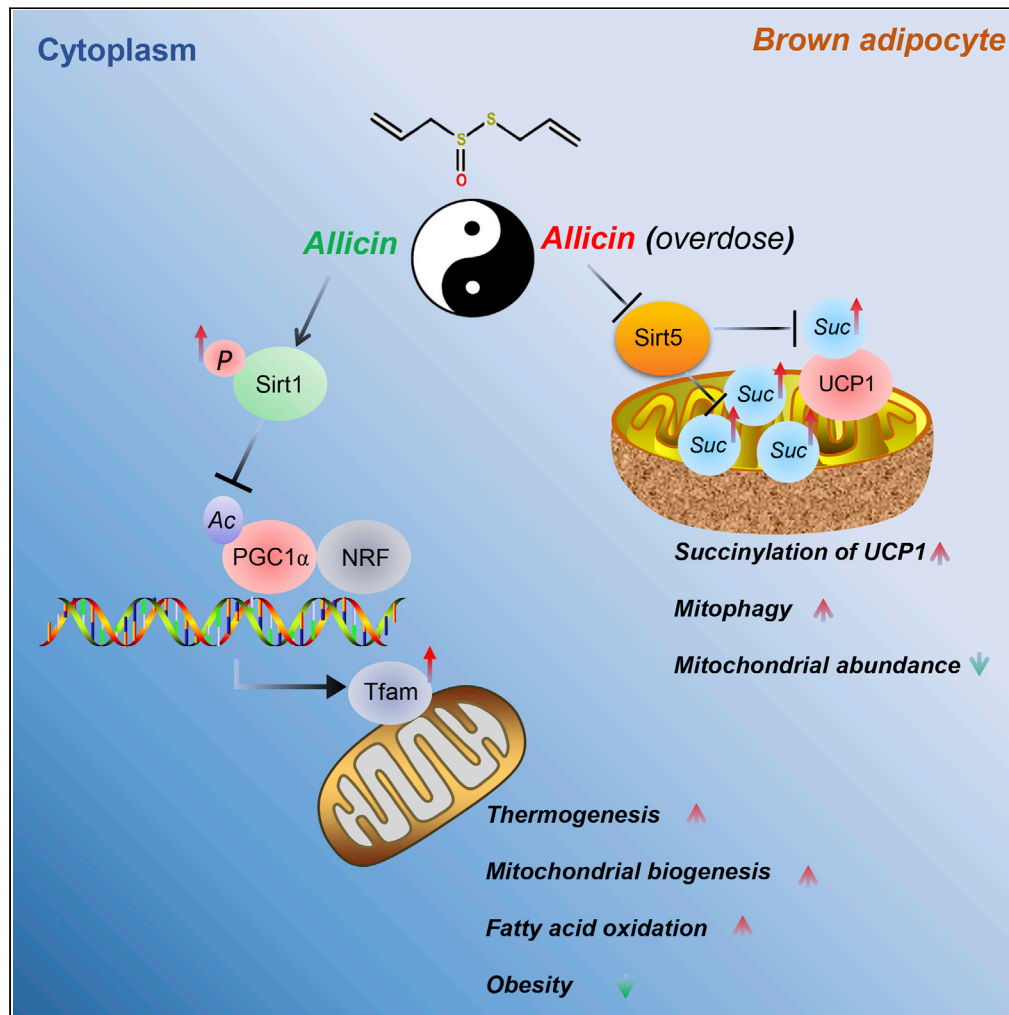**Article**

Allicin Regulates Energy Homeostasis through Brown Adipose Tissue

Chuanhai Zhang, Xiaoyun He, Yao Sheng, ..., Wentao Xu, Yunbo Luo, Kunlun Huang

lyb@cau.edu.cn (Y.L.)
hkl009@163.com (K.H.)

HIGHLIGHTS

Allicin reduces adiposity and maintains glucose homeostasis

Allicin activates the brown adipocytes and increases the energy expenditure

Allicin enhances BAT activity partly through SIRT1-PGC1a-Tfam signaling pathway

Allicin regulates mitophagy via suppressed sirt5-mediated succinylation accumulation

Article

Allicin Regulates Energy Homeostasis through Brown Adipose Tissue

Chuanhai Zhang,[1,2] Xiaoyun He,[1,2] Yao Sheng,[1,2] Jia Xu,[1,2] Cui Yang,[1,2] Shujuan Zheng,[1,2] Junyu Liu,[1,2] Haoyu Li,[1,2] Jianbing Ge,[1,2] Minglan Yang,[1,2] Baiqiang Zhai,[1,2] Wentao Xu,[1,2] Yunbo Luo,[1,2,*] and Kunlun Huang[1,2,3,*]

SUMMARY

Brown adipose tissue (BAT) is a promising potential therapeutic target for the treatment of obesity and related metabolic diseases. Allicin, a natural product in garlic, has multiple biological and pharmacological functions. However, the role of allicin in the regulation of metabolic organs, particularly BAT activation, has not been well studied. Here, we show that allicin imparts a significant effect by inhibiting body weight gain, decreasing adiposity, maintaining glucose homeostasis, improving insulin resistance, and ameliorating hepatic steatosis in obese mice. These observations strongly correlate with the activation of BAT. Notably, allicin plays a role in BAT activation, which may partly contribute to the Sirt1-PGC1α-Tfam pathway. In addition, allicin can significantly increase the succinylation levels of UCP1 in BAT by inhibiting sirt5, whereas excess allicin induces autophagy/mitophagy and mitochondrial dysfunction. Thus, our findings point to allicin as a promising therapeutic approach for the treatment of obesity and metabolic disorders.

INTRODUCTION

The regulation of energy homeostasis, including food intake, energy expenditure, and body adiposity, is crucial to a healthy body (Murphy and Bloom, 2006; Farooqi and O'Rahilly, 2005). Obesity is the result of an imbalance in energy homeostasis, which is caused by energy intake that exceeds energy expenditure, and excess energy is stored in fat in the form of triglycerides (TGs), leading to adiposity (Yuan et al., 2017) and causing a series of metabolic diseases, such as insulin resistance, type 2 diabetes mellitus, cardiovascular disease, cancer, inflammation, and other related diseases (Yin et al., 2019). At present, obesity has become one of the fastest-growing non-communicable diseases, and global estimates have shown that by 2030, 38% adults would be overweight and 20% will develop obesity (Nishtar et al., 2016; Geserick et al., 2018). Although obesity is dire, satisfactory, safe, and effective treatment strategies are limited.

There are two main types of fat in mammals, namely, energy-storing white adipose tissues (WAT) and energy-consuming brown adipose tissues (BATs) (Peirce et al., 2014). Unlike WAT, BAT contains a large number of mitochondria, which is responsible for nonshivering thermogenesis in mammals (Zhang et al., 2016; Cannon and Nedergaard, 2004). Several studies have shown that the potential therapy of anti-obesity and related metabolic diseases is related to the activation of BAT (Harms and Seale, 2013; Matsushita et al., 2014; Kajimura et al., 2015; Zhou et al., 2018). Furthermore, proper stimulus could induce the generation of uncoupling protein-1 (UCP1) in WAT, which is also rich in mitochondria and defined as beiging (Wu et al., 2012). Many studies have suggested that beiging in WAT can also effectively enhance energy expenditure and improve metabolic disorders (Boström et al., 2012; Seale et al., 2011). Furthermore, reducing the amount of WAT and the size of white adipocytes can effectively improve inflammation and metabolic disorders (Merrick et al., 2019). Both WAT and BAT have essential functions in regulating energy homeostasis. Therefore, increasing BAT activation and inducing beiging in WAT could be an effective therapeutic strategy for obesity and related diseases.

SIRT1, a nuclear NAD$^+$-dependent protein deacetylase (Landry et al., 2000) that belongs to the sirtuin family (referred to as Sirt1 to Sirt7) (Frye, 2000), plays a vital role in regulating transcription in various key metabolites (Zhang et al., 2018). Many studies have reported that SIRT1 can enhance BAT function and

[1]Beijing Advanced Innovation Center for Food Nutrition and Human Health, College of Food Science and Nutritional Engineering, China Agricultural University, Beijing 100083, China

[2]Key Laboratory of Safety Assessment of Genetically Modified Organism (Food Safety), Ministry of Agriculture, Beijing 100083, China

[3]Lead Contact

*Correspondence: lyb@cau.edu.cn (Y.L), hkl009@163.com (K.H.)

https://doi.org/10.1016/j.isci.2020.101113

regulate metabolism (Xu et al., 2013; Boutant et al., 2015; Chalkiadaki and Guarente, 2012). PGC1α is an essential regulator of mitochondrial biogenesis (Lagouge et al., 2006) that can co-activate nuclear respiratory factor-1 (NRF-1) activity at the TFAM promoter. Several studies have shown that sirt1 can regulate mitochondrial function by regulating PGC-1α and NRF pathway activity (Lagouge et al., 2006; Yuan et al., 2017; Du et al., 2011). Furthermore, Sirt5, another member of the sirtuin family, which is located in mitochondria, plays an essential role in desuccinylase activity (Rardin et al., 2013). Recent studies have shown that sirt5 regulates the mitochondrial lysine succinylome (Wang et al., 2019) and has major regulatory effects on BAT function and UCP1 activity through succinylation modification (Shuai et al., 2019). It has also been reported that sirt5 regulates the differentiation of brown adipocytes and browning of subcutaneous fat (McRae, 2005). However, the regulation and function of succinylation in different tissues and organs remain unclear. More importantly, studies on the regulatory role of small molecules on sirt5 and succinylation are limited.

Emerging evidence suggests that mitophagy/autophagy plays an essential role in the physiology of the mitochondria-enriched brown and beige adipocytes, which also suggests that elucidation of the molecular links between mitophagy/autophagy and energy metabolism may facilitate in the identification of potential targets for the treatment of obesity and related metabolic disorders (Liesa and Shirihai, 2013; Ro et al., 2019). Mitophagy pertains to the selective removal of mitochondria through autophagy, which is driven by specific proteins (e.g., BNIP, FUNDC1, NIX, and BCL2L13) interacting with autophagosomal protein LC3 that drives autophagosomes and degrades its contents and is usually employed as a common marker of autophagy (Altshuler-Keylin and Kajimura, 2017). Furthermore, LC3II/LC3I is often used as the activation marker of autophagy (Li et al., 2019). Damage to the mitochondria is a major physiological trigger for mitophagy. Given the vital role of the mitochondria in the thermogenic function of brown and beige adipocytes, it is significant to investigate the mechanisms underlying the regulation of mitophagy/autophagy in thermogenic fat organs.

Allicin, the main bioactive ingredient in garlic (Chan et al., 2013), has multiple pharmacological functions, including anti-oxidative stress, anti-tumor and cholesterol-lowering effects, anti-platelet aggregation, liver protection, prevention of cardiovascular disease, and anti-inflammatory capacity (Ding et al., 2016; El-Sheakh et al., 2016; Lee et al., 2019). Although allicin induces beiging in WATs (Chi and Wang, 2011), its effect on the regulation of energy homeostasis, including whole-body energy metabolism, and the mechanism of activation of BAT of allicin remains unclear. In this study, we determined the effect of allicin on whole-body energy metabolism and BAT activation and its underlying mechanism. Our results showed that allicin significantly induces the activity of the Sirt1-Pgc1α-Tfam signaling cascade and increases the generation of mitochondria in BAT. Importantly, we propose that allicin is a potential agonist of succinylation and plays a vital role in the regulation of UCP1 activity and that excessive garlic intake could impair BAT function due to the allicin-induced mitophagy in brown adipocytes. Our findings establish that allicin plays a previously not fully recognized role in regulating energy homeostasis, which may facilitate the development of a novel therapeutic approach for the treatment of metabolic disorders.

RESULT

Allicin Reduces Adiposity and Maintains Glucose Homeostasis in Mice

To investigate the effect of allicin on energy homeostasis, high-fat-diet (HFD)-induced obesity and genetically leptin-receptor-deficient obese (Db/Db) mouse models were used to assess the role of allicin on obesity and energy metabolism. First, we screened the optimal treatment concentration (allicin-high 1 mg/mL, which means allicin was consumed about 4.2 mg/day per mice) of allicin by observing the effect of three doses of allicin on the reduction of body weight of HFD mice (Figures 1A and S1B) and then treated Db/Db mice with the optimal concentration. A significant reduction in body weight after allicin treatment was observed both in HFD and Db/Db mouse models (Figures 1A, 1B, and S2A–S2C). The protection from weight gain after allicin treatment was mainly due to the reduction in fat accumulation in epididymal WAT (eWAT) and subcutaneous WAT (sWAT) (Figures 1C–1F, S2D, and S2E). These findings indicate that the anti-adiposity effect of allicin is evident from long-term accumulations of both innate and genetic obesity. Adiposity often affects glucose homeostasis, so glucose homeostasis and insulin resistance were analyzed by glucose tolerance test and insulin tolerance test in HFD and Db/Db mice. As expected, allicin treatment improved glucose tolerance and insulin responses (Figures 1G–1J, S2F, and S2G). Furthermore, serum profiles, including total cholesterol (CHO), TG, low-density lipoprotein (LDL), and nonesterified fatty acid
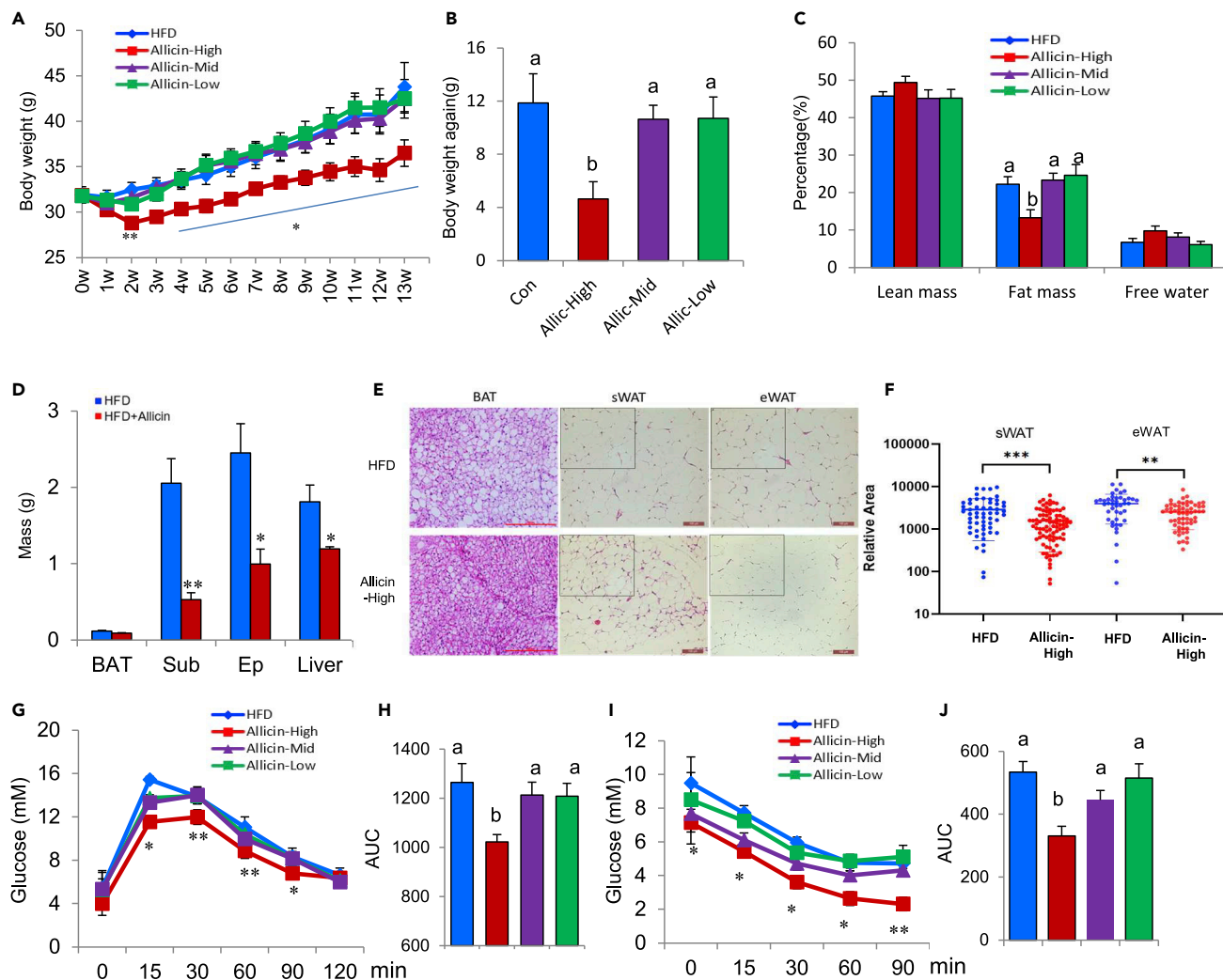
Figure 1. Allicin Reduces Adiposity and Improves Glucose Homeostasis in DIO Mice

Vehicle (control) or different doses of allicin were administrated each day for a total of 13 weeks.

(A) Body weight evaluation of control HFD mice or mice treated with different doses of allicin. (n = 9).

(B) Body weight again of different groups of mice (n = 9).

(C) Body fat percentage test using nuclear magnetic resonance.

(D) Organ weight of control and allicin-treated HFD mice (n = 6).

(E) H&E staining of BAT, sWAT, and eWAT sections from DIO control and allicin-treated DIO mice. Scale bars, 100 μm.

(F) Quantification of the area of adipocytes in the selection of H&E sections in (E).

(G and H) (G) Glucose tolerance test of control and allicin-treated DIO mice (intraperitoneally with glucose as 1.0 g/kg after 16-h fast) (n = 8). (H) The average area under the curve (n = 8).

(I and J) (I) Insulin tolerance test was performed on control and allicin-treated DIO mice (injection insulin with 2.0 U/kg after 6 h of fasting (n = 8). (J) The average area under the curve (n = 8).

Values represent means ± SEM. Error bars represent SEM; significant differences compared with vehicle controls are indicated by *p < 0.05, **p < 0.01(assessed by Student's t test). Different letters indicate signicance among groups (P<0.05).

(NEFA) levels, also markedly decreased after allicin treatment in DIO mice (Figure S3). Taken together, these results indicate that allicin notably ameliorates adiposity and maintains glucose homeostasis in mice.

Allicin Augments Whole-Body Energy Expenditure by Activation of Brown Adipose Tissue

Energy consumption is an essential indicator of energy homeostasis. We next investigated the effect of allicin on whole-body energy expenditure in HFD and Db/Db mice using the respiratory metabolic system. We found that allicin markedly increased oxygen consumption in both HFD and Db/Db mice
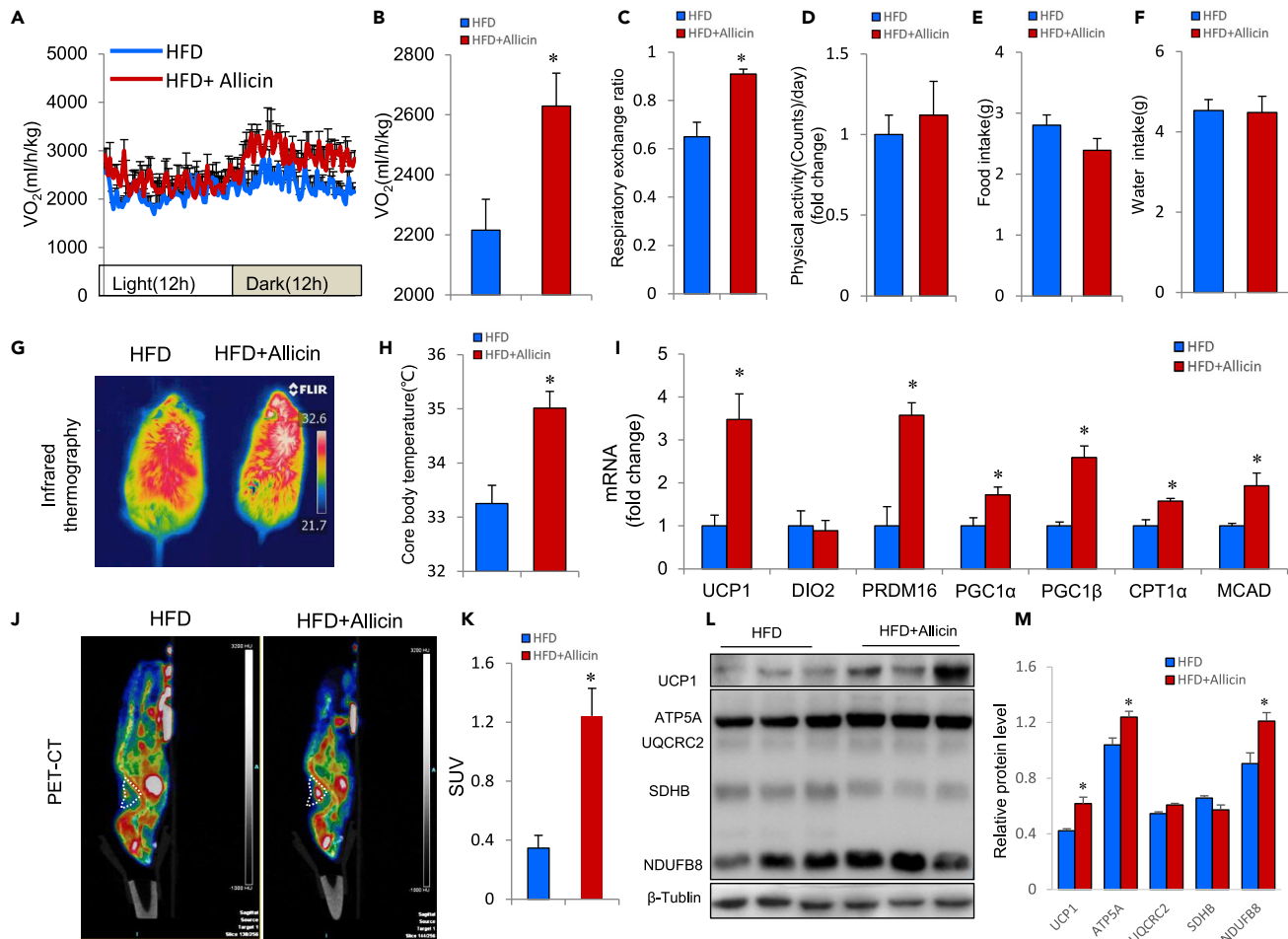
Figure 2. Allicin Increases Energy Expenditure and Enhances BAT Activity in DIO Mice

(A–F) (A and B) Energy expenditure was assessed by oxygen consumption (VO2) in DIO mice after 12 weeks of allicin treatment (B) (n = 5); (C–F) respiratory exchange ratio (C), physical activity (D), food intake (E), and water intake (F) of control and allicin-treated DIO mice (n = 5).

(G) Infrared thermal images of control and allicin-treated DIO mice, which shows more thermal signals in the interscapular BAT position.

(H) The core body temperature of control and allicin-treated mice after cold stimulation (4°C for 4 h).

(I) The real-time PCR analysis of thermogenic genes in BAT from control and allicin-treated DIO mice.

(J–L) (J and K) PET/CT images after injection of 18F-fluorodeoxyglucose (18F-FDG) into DIO mice treated with vehicle and allicin for 12 weeks (J). White triangles indicate the anatomical site of the interscapular BAT (n = 3). Mean standard uptake value (SUV) of 18F-FDG in BAT (K). UCP1 and OXPHOS expression levels in BAT of control and allicin-treated DIO mice (L).

(M) The relative protein levels of (L).

Values represent the means ± SEM. Error bars represent SEM; significant differences compared with vehicle controls are indicated by *p < 0.05 (assessed by Student's t test).

(Figures 2A–2C, S4A, and S4B), indicating that the allicin-treated group has a higher energy expenditure. However, no significant difference in physical activity, food intake, or water intake was observed (Figures 2D-2F, and S4C). Allicin treatment also significantly increased thermogenesis in interscapular BATs and rectal temperature after cold stimulation compared with the control HFD and Db/Db mouse groups (Figures 2G, 2H, S4D, and S4E). BAT is well known as an essential thermogenic and energy-consuming organ in the body; it maintains body temperature by non-shaking thermogenesis with cold stimuli. Based on the above-mentioned results, we hypothesized that allicin augments whole-body energy expenditure by activating BAT in HFD and Db/Db mice. Allicin treatment also significantly induced the expression of genes related to thermogenesis and energy expenditure, including Ucp1, Prdm16, Pgc1α/β, Cpt1α, and Mcad, in the BAT from HFD mice (Figure 2I). Meanwhile, 18F-fluorodeoxyglucose positron emission tomography (PET) combined with X-ray computed tomography (CT) analysis show that allicin treatment dramatically increased the glucose utilization rate in both HFD and Db/Db mice (Figures 2J, 2K, S4F, and S4G).

Histological analysis of BAT indicates that allicin treatment reduces the size of lipid droplets (Figures 1F and S3H). Immunoblotting analysis further indicated that allicin significantly enhances expression of UCP1 and OXPHOS-related proteins (ATP5A and NDUFB8) in BAT of both HFD and Db/Db mouse (Figures 2L, 2M, and S3I). These results strongly indicate that allicin dramatically increases BAT activity in HFD and Db/Db mice. These results together confirm that allicin treatment increases whole-body energy expenditure and reduces adiposity in mice.

To further confirm that the anti-obesity role of allicin is mainly via regulation of BAT activation, allicin treatment was performed on diet-induced obese mice under thermoneutral condition (28°C–30°C), which will make BAT inactive. The results showed that allicin treatment did not significantly reduce body weight gain under thermoneutral conditions (Figures S5A and S5B), with no difference in food and water intake (Figures S5C and S5D). In addition, thermogenesis in the mice also did not exhibit any significant improvement (Figures S5E and S5F) and the morphology of BATs did not show any activation phenotype (Figure S5G) after allicin treatment. Simultaneously, allicin treatment did not significantly improve the fatty liver after loss of BAT activity (under thermoneutral conditions) in DIO mice. These results clearly indicate that the anti-obesity role of allicin depends more on BAT activation.

Allicin Activates the Brown Adipocytes and Increases the Energy Expenditure *In Vitro*

The above-mentioned results have proved that allicin increases energy expenditure via activation of BAT *in vivo*. However, whether allicin activates brown fat as a direct or indirect effect remains unclear. To resolve this question, we isolated brown primary adipocytes from mice and performed an *in vitro* brown adipocyte differentiation assay with or without allicin treatment. The results showed that allicin increases the expression of UCP1, which is the golden marker of BAT activation, in a dose-dependent manner and with the best activation effect at a concentration of 50 μM (Figure 3A). In addition, the thermogenic genes, including PGC1α/β and CPT1α/β, were also upregulated after allicin treatment compared with solvent treatment (Figure 3B). Furthermore, UCP1 levels were further confirmed by quantification of protein expression by immunostaining and immunoblotting (Figures 3C–3E). Furthermore, the expression levels of the OXPHOS proteins, including ATP5A, UQCRC2, SDHB, and NDUFB8, were markedly upregulated after allicin treatment compared with solvent treatment (Figure 3D-3E). Importantly, the effect of allicin on energy expenditure was assessed based on the oxygen consumption rate (OCR) in brown adipocytes. As expected, the OCR-related basal metabolic rate, ATP levels, maximum oxygen consumption, and proton leakage all markedly increased after allicin treatment compared with solvent treatment (Figures 3F–3J). We also investigated the effect of allicin on the activation of human brown adipocytes. Surprisingly, the expression levels of thermogenic genes, including UCP1, PGC1α/β, and CPT1α/β, dramatically increased after brown adipocyte differentiation cocktail medium treatment with allicin compared with solvent treatment (Figure S6A). The expression of mitochondrial biogenic transcription factors, including NRF1, NRF2, and TFAM, were markedly upregulated in human brown adipocytes after allicin treatment (Figure S6B). Simultaneously, the mitochondrial copy number was obviously increased in human brown adipocytes after treatment with allicin (Figure S6C). Furthermore, the UCP1 levels in human brown adipocytes were further confirmed by immunoblotting and immunostaining (Figures S6D and S6E). Meanwhile, the expression levels of OXPHOS proteins in human brown adipocytes also were significantly upregulated after allicin treatment compared with solvent treatment (Figure S6E). The results of human brown adipocytes indicated that allicin may be potentially utilized in the treatment of human metabolic diseases. Collectively, these results indicate that allicin can activate brown adipocytes and increase energy expenditure *in vitro*.

Allicin Induces Beiging in Subcutaneous WAT

Both BAT and WAT play important roles in maintaining energy homeostasis. Based on the above-mentioned findings (Figures 1–3), we hypothesized that allicin also could induce the activation of UCP1 in sWAT, i.e., it contributes to the induction of beiging in sWAT. First, we evaluated the expression level of the beige markers in sWAT of HFD and Db/Db mice. Interestingly, the mRNA levels of beige cell-specific markers, such as CD137, TMEM26, and TBX1, significantly increased in sWAT of HFD and Db/Db mice (Figures S7A and S7D). Furthermore, thermogenic and fatty acid oxidation-related genes, such as UCP1, PRDM16, PGC1α/β, and CPT1α, were significantly upregulated in sWAT after allicin treatment (Figures S7C and S7F). Beige cells also contain abundant mitochondria, similar to classical brown adipocytes. Thus, we next investigated the expression of mitochondrial biogenic transcription factors, including TFAM, NRF1, and NRF 2, and we found that their expression levels were markedly upregulated after allicin treatment (Figures S7B and S7E). Importantly, we also investigated the effect of allicin on the induction of
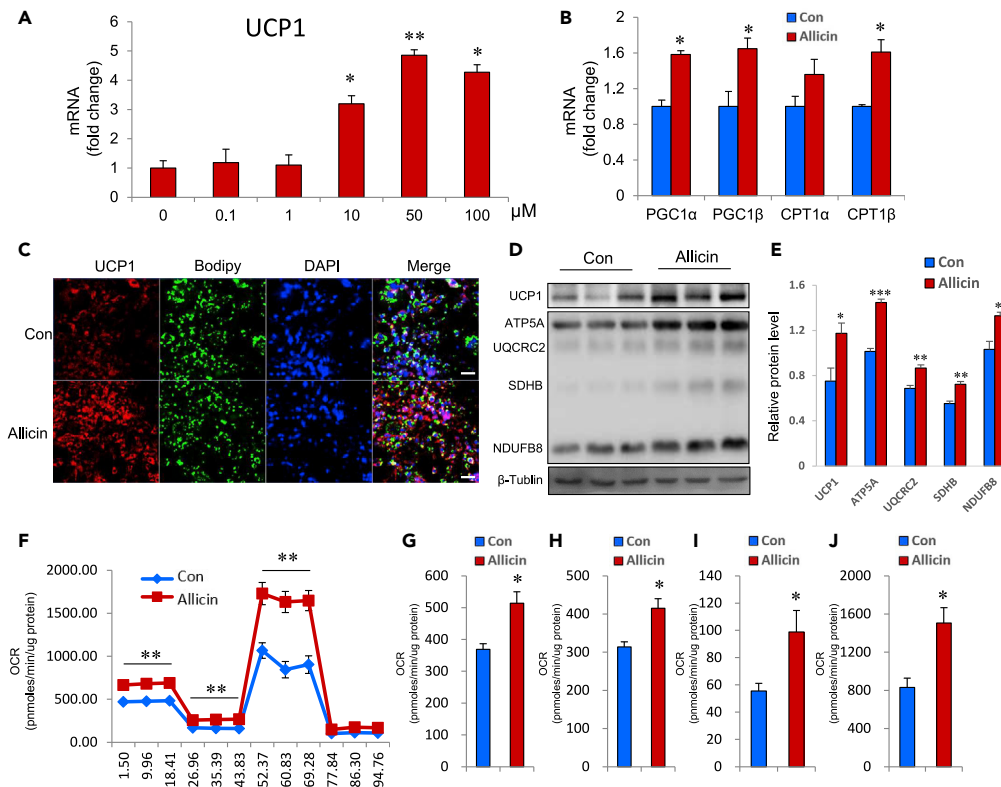
Figure 3. Allicin Increases the Activity of Brown Adipocytes and Oxygen Consumption *In Vitro*

(A) Dose-dependent effect of allicin on UCP1 expression in primary brown adipocytes on day 6 of brown adipogenesis.

(B) Thermogenic gene expression in brown adipocytes treated with 50 μM allicin or DMSO.

(C) Immunofluorescence staining of UCP1 and BODIPY in brown adipocytes treated with 50 μM rutin or DMSO at day 6 of brown adipogenesis. Scale bars, 50 μm.

(D–E) The protein levels of UCP1 and OXPHOS in brown adipocytes treated with DMSO or Allicin.

(F) Oxygen consumption rates (OCR) at day 6 of brown adipogenesis with Allicin or DMSO treatment. (n = 5).

(G–J) The OCR-related basal metabolic rate(G), ATP levels(H), maximum oxygen consumption(I), and proton leakage(J). (n = 5).

Values represent means ± SEM. Error bars represent SEM; significant differences compared with vehicle controls are indicated by *p < 0.05, **p < 0.01, ***p < 0.001 (assessed by Student's t test).

beiging in human white adipocytes. Surprisingly, the expression of beiging marker genes, such as CD137, TMEM26, and TBX1, significantly increased in human white adipocytes after brown adipocyte differentiation cocktail medium treatment with allicin (Figure S8A). Moreover, the expression levels of thermogenic genes, including UCP1, PGC1α/β, and CPT1α/β, were markedly upregulated after brown adipocyte differentiation cocktail medium treatment with allicin (Figure S8B). Also, the mitochondrial copy number was obviously increased in beige adipocyte after treatment with allicin (Figure S8C). The UCP1 levels were further confirmed by immunostaining and immunoblotting (Figures S8D and S8E). The expression levels of OXPHOS proteins also significantly increased after allicin treatment (Figure S8E). These results suggest that allicin treatment may improve energy consumption by increasing beige cell formation.

Allicin Relieves Hepatic Steatosis

Obesity caused by an imbalance of energy homeostasis often leads to hyperlipidemia and fatty liver. Therefore, we investigated whether allicin mediates fat reduction by preventing hyperlipidemia and hepatic steatosis in HFD and Db/Db mice. The liver mass of HFD mice markedly decreased after allicin treatment (Figure 1D). Morphology analysis also showed that liver size is smaller and the color of the liver is more biased toward normal in HFD and Db/Db mice after allicin treatment (Figure 4A). Histological analysis of H&E and oil red O staining showed that allicin treatment dramatically reduced the lipid accumulation in the liver of HFD and Db/Db mice (Figure 4A). In addition, TG content analysis showed that allicin treatment strongly inhibited liver lipid
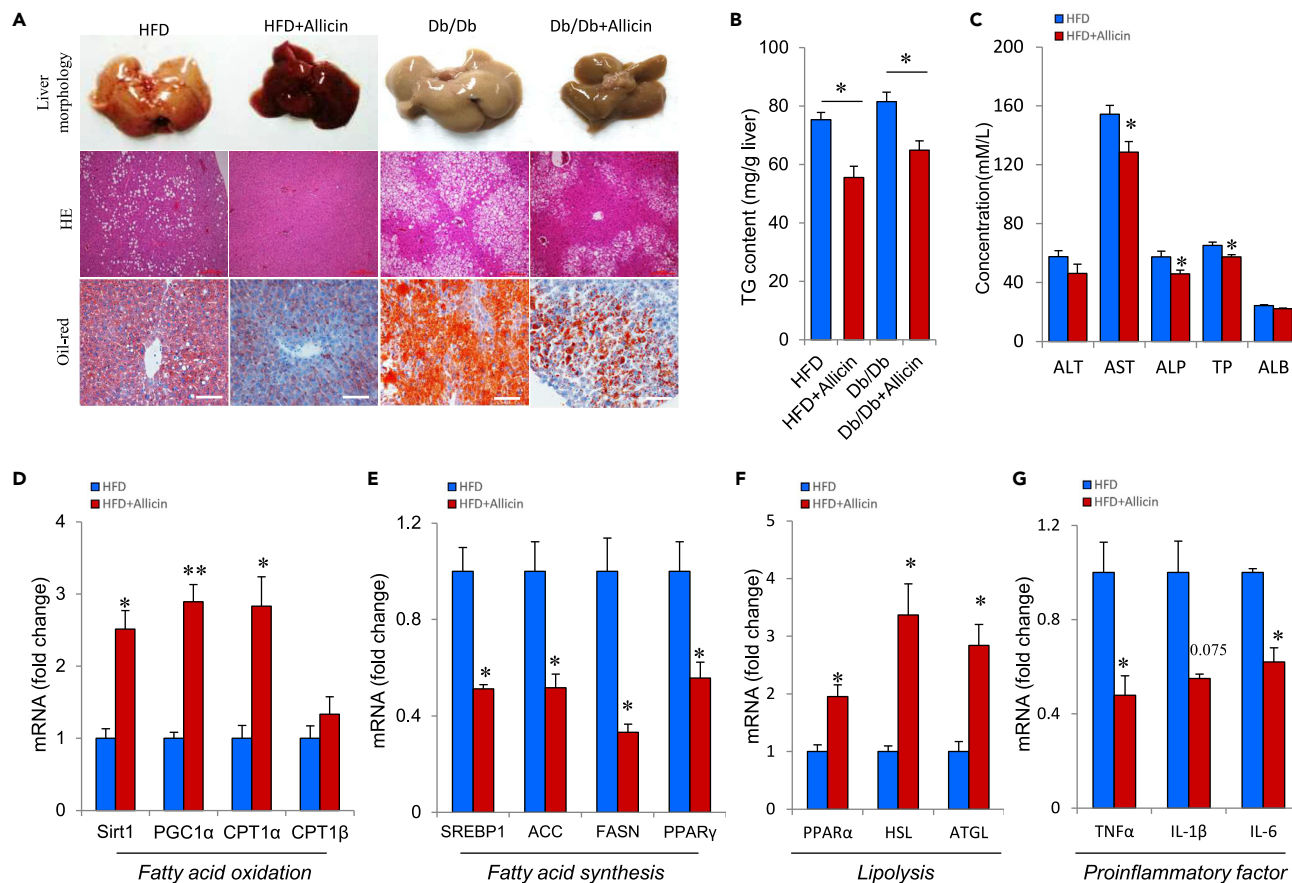
Figure 4. Allicin Relieves Hepatic Steatosis in Obese Mice

(A) Liver morphology and H&E and oil red O staining from liver sections in control and allicin-treated DIO mice and Db/Db mice. Scale bars, 100 μm.

(B) TG concentrations in the liver of DIO mice and Db/Db mice.

(C) Serum aspartate aminotransferase (AST), alanine aminotransferase (ALT), alkaline phosphatase (ALP), total protein (TP), and albumin (ALB) levels in control and allicin-treated DIO mice.

(D–G) (D–F) Real-time PCR analysis of fatty acid oxidation-related gene (D), fatty acid synthesis-related gene (E), lipolysis-related genes (F), and inflammatory factor-related genes (G) in the liver of control and allicin-treated DIO mice.

Values represent the means ± SEM. Error bars represent SEM; significant differences compared with vehicle controls are indicated by *p < 0.05, **p < 0.01 (assessed by Student's t test).

accumulation and ameliorated liver steatosis in obese mice (Figure 4B). Furthermore, the plasma levels of aspartate aminotransferase, alkaline phosphatase, and total protein markedly decreased and were closer to normal values in obese mice after allicin treatment (Figure 4C). Serum profiles, including CHO, TG, LDL, and NEFA levels, also markedly decreased in HFD mice after Allicin treatment (Figure S3). The expression levels of fatty acid oxidation-related genes (*Sirt1, PGC1α, CPT1,* and *CPT1β*) and lipolysis-related genes (*PPARα, HSL,* and *ATGL*) significantly increased, whereas those of fatty acid synthesis (*SREBP1, ACC, FASN,* and *PPARγ*) and proinflammatory (*TNFα, IL1β,* and *IL6*) factors markedly decreased in HFD mice after allicin treatment (Figures 4D–4G). These findings indicate that allicin activates BATs and improves whole-body energy metabolism, thereby improving hepatic steatosis. However, allicin treatment did not significantly improve hepatic steatosis after losing BAT activity (under thermoneutral conditions) in DIO mice. In summary, these results indicate that allicin specifically attenuates hepatic steatosis, and BAT plays an important role in positively regulating whole-body energy metabolism in obese mice.

Allicin Enhances the Activity of SIRT1 and Activates the Downstream PGC1α-Tfam Signaling Pathway

As shown in the previous sections, allicin upregulates sirt1 levels in the liver of obese mice. Sirt1-mediated PGC1α deacetylation and activation are essential for the generation and function of mitochondria (Yuan
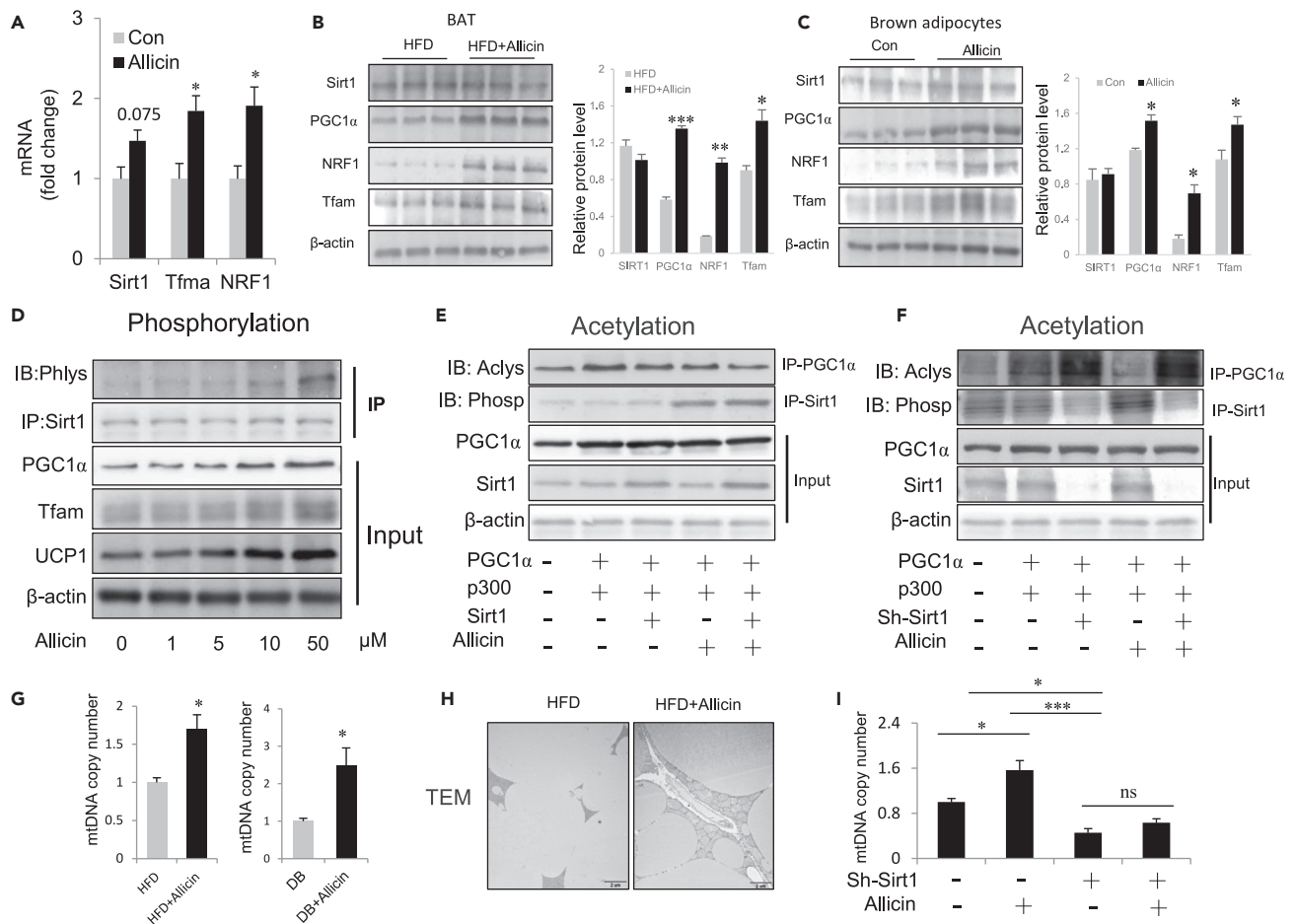
Figure 5. Allicin Promotes Mitochondrial Biogenesis through the Activation of Sirt1-PGC1α-Tfam Pathway

(A) The mRNA expression of SIRT1, Tfam, and NRF1 in BAT from control and allicin-treated DIO mice.

(B) Western blot analysis of the Sirt1, PGC1α, NRF1, and Tfam in BAT from control and allicin-treated DIO mice.

(C) Western blot analysis of Sirt1, PGC1α, NRF1, and Tfam in brown adipocytes treated with or without allicin.

(D) The phosphorylation levels of sirt1 in brown adipocytes treated with allicin at different concentrations.

(E) SIRT1 deacetylates PGC1α, and allicin treatment substantially increases the phosphorylation of sirt1 and SIRT1-mediated PGC1α deacetylation.

(F) In contrast, shSIRT1 treatment significantly diminishes allicin-mediated PGC1α deacetylation.

(G) Mitochondrial mtDNA copy number in BAT from control and allicin-treated DIO or Db/Db mice.

(H) Transmission electron microscopic (TEM) analysis of mitochondrial in BAT of control and allicin-treated DIO mice. Scale bars, 2 μm.

(I) shSIRT1 treatment significantly diminishes the allicin-mediated increase in mtDNA copy number. Values represent means ± SEM. Error bars represent SEM; significant differences compared with vehicle controls are indicated by *$p < 0.05$, **$p < 0.01$, ***$p < 0.001$ (assessed by Student's t test).

et al., 2017). These clues prompted us to hypothesize that allicin-induced BAT activation occurs via the Sirt1-PGC1α signaling pathway. Therefore, we next investigated the expression of sirt1 in BATs of HFD mice treated with or without allicin. The results showed that the expression levels of sirt1 did not significantly change with allicin treatment (Figures 5A and 5B). However, the downstream proteins of sirt1, including PGC1α, NRF1, and Tfam, which belong to the PGC1α-Tfam signaling pathway, were significantly upregulated after allicin treatment (Figures 5A and 5B). These results also confirm the findings of allicin treatment in brown adipocytes in vitro (Figure 5C). As is known, protein phosphorylation is an important post-translational modification that regulates protein activity. We next investigated the phosphorylation level of sirt1 through immunoprecipitation experiments in brown adipocytes treated with allicin using a phosphorylated pan-antibody. Interestingly, the phosphorylation level of sirt1 increased in a dose-dependent manner and coincided with the internal protein expression levels of PGC1α, Tfam, and UCP1 (Figure 5D). These results indicate that allicin influences SIRT1 activity by enhancing the phosphorylation levels of Sirt1. Then, we further investigated whether allicin regulates Sirt1 activity and the downstream PGC1α-
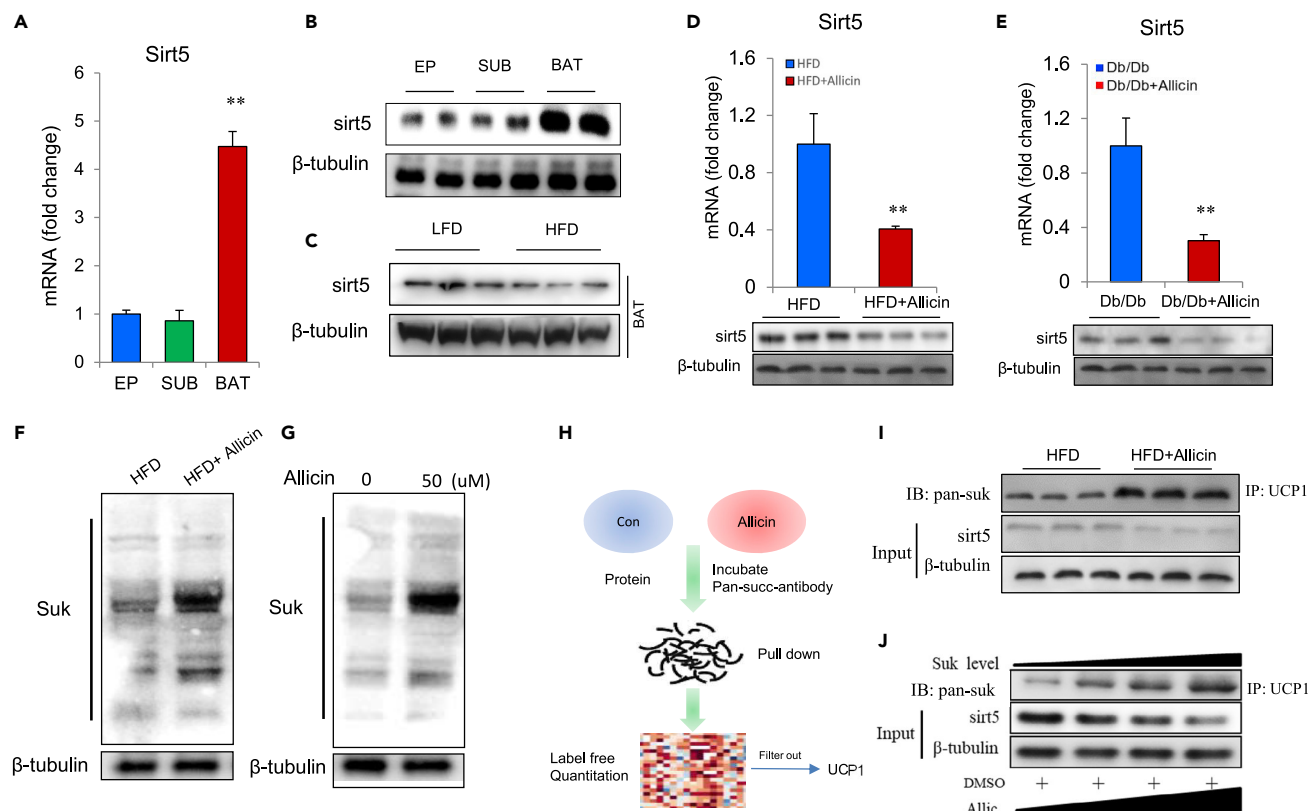
Figure 6. Allicin Upregulates Succinylation Levels in BAT by Inhibiting sirt5

(A and B) Sirt5 expression levels in eWAT, sWAT, and BAT in mice.

(C and D) (C) The protein expression levels of Sirt5 in BAT in low-fat diet and HFD mice. (D) Sirt5 expression levels in BAT from control and allicin-treated DIO mice.

(E) Sirt5 expression levels in BAT from control and allicin-treated Db/Db mice.

(F) Protein succinylation levels in BAT from control and allicin-treated DIO mice.

(G) The protein succinylation levels in brown adipocytes treated with or without allicin.

(H) Schematic diagram of the process of label-free proteomic analysis.

(I) Allicin treatment increases the succinylation levels of UCP1 in brown adipocytes by immunoprecipitation analysis.

(J) Succinylation levels of UCP1 increase in brown adipocyte after allicin treatment and in a dose-dependent fashion. Values represent means ± SEM. Error bars represent SEM; significant differences compared with vehicle controls are indicated by **$p < 0.01$ (assessed by Student's t test).

Tfam signaling pathway in vitro. SIRT1 deacetylates PGC1α (Figure 5E). Importantly, allicin treatment substantially enhances the phosphorylation of sirt1 and increases Sirt1-mediated PGC1α deacetylation (Figure 5E). Conversely, knocking down Sirt1 weakens Allicin-mediated PGC1α deacetylation (Figure 5F). These results indicate that allicin increases SIRT1 deacetylase activity by enhancing its phosphorylation. Furthermore, we assessed the generation of mitochondria by analyzing mtDNA copy number and transmission electron microscopy (TEM). As expected, allicin treatment dramatically increased the number of mitochondria in BAT, as evidenced by mtDNA copy number analysis (Figure 5G) and TEM examination (Figure 5H). In addition, the absence of sirt1 inhibited the allicin-mediated increase in mtDNA copy number (Figure 5I). Collectively, these findings prove that allicin improves mitochondrial generation by activating SIRT1 and the downstream PGC1α-Tfam signaling pathway in BATs.

Allicin Enhances Succinylation of UCP1

As mentioned earlier, sirt5 also plays critical regulatory roles in BAT function and UCP1 activity via succinylation modification (Wang et al., 2019). However, available information on the regulation of succinylation by small molecules in food is limited. Therefore, we investigated the effect of allicin on succinylation in BATs. First, we examined the expression levels of desuccinylase-sirt5 in different adipose tissues and found that sirt5 is most abundant in BATs compared with the other two adipose tissue (Figures 6A

and 6B). This indicated that BAT may be the main target organ of succinylation in adipose tissues. Furthermore, sirt5 was downregulated in the BATs of HFD mice compared with low-fat diet mice (Figure 6C), which suggests that sirt5 plays important role in BAT function during diet-induced obesity. We next found that allicin treatment markedly decreased the mRNA and protein expression levels of sirt5 both in HFD and Db/Db mice (Figures 6D and 6E). This result indicates that allicin treatment enhances the succinylation levels of certain proteins in BAT. Furthermore, immunoblotting analysis using a pan-succinylation antibody indicates that allicin treatment increases the succinylation levels of various proteins in BATs and brown adipocytes (Figures 6F and 6G). At this point, we wanted to determine which proteins had undergone succinylation modification. Surprisingly, we identified the changed succinylation levels of UCP1 from a series of pulled-down proteins in BATs through label-free proteomics analysis of allicin-treated and HFD control mice (Figure 6H). Then, we further confirmed that the succinylation levels of UCP1 significantly increase after allicin treatment of brown adipocytes (Figure 6I). Furthermore, the increase in succinylation levels of UCP1 depends on the dosage of allicin both in mouse and human brown adipocytes (Figures 6J and S6F).

Excess Allicin Induces Mitophagy in Brown Adipocytes

Allicin treatment also upregulates succinylation-related proteins in a concentration-dependent manner (Figure 7A). These results suggest that allicin may be an activator of succinylation. Previous reports have indicated that the excessive accumulation of succinylation results in impairment of BAT function (Wang et al., 2019). This implies that allicin treatment using excessive amounts may cause BAT dysfunction. Dose-dependent allicin treatment of brown adipocytes results in the gradual deterioration of cell morphology, whereas the level of succinylation of proteins gradually increased (Figures 7A and 7B). Meanwhile, the mRNA expression levels of UCP1 gradually decreased with increasing allicin concentrations, particularly after exceeding the optimal concentration (Figure 7C). Moreover, treatment with excessive amounts of allicin (500 μM) triggered the expression of autophagy/mitophagy markers, whereas diminished the expression of mitochondrial Oxphos-related genes in brown adipocytes (Figures 7D and 7E). Notably, allicin treatment using a moderate concentration (50 μM) did not induce the expression of autophagy/mitophagy markers, but it dramatically stimulated the expression of mitochondrial Oxphos-related genes (Figures 7D and 7E). These results suggest that treatment with excessive amounts of allicin may induce mitophagy, impair mitochondrial homeostasis, and decrease the number of mitochondria in brown adipocytes. LC3II/LC3I is a biomarker of autophagy activation. Interestingly, we found that treatment with excessive amounts of allicin promotes autophagy/mitophagy and decreases the number of mitochondria. Conversely, Sirt5 overexpression can partly rescue these phenotypes (Figures 7F and 7G). This indicated that excessive amounts of allicin induce mitochondrial dysfunction partly through the suppressed sirt5-mediated succinylation accumulation in brown adipocytes. All the above-mentioned results suggest that allicin has dual functions, and treatment with excessive amounts may disrupt energy homeostasis. Although allicin imparts a positive effect on regulating energy homeostasis, treatment with excessive amounts may lead to a disorder of energy metabolism due to the dysfunction of BAT. Our findings thus provide useful information and theoretical basis for the rational use of allicin as a safer, more effective, and valuable molecule for the treatment of metabolic diseases.

DISCUSSION

Metabolic diseases caused by the imbalance in energy homeostasis are collectively considered as epidemics, particularly obesity and related metabolic diseases. BAT is a critical organ that regulates energy homeostasis and is known as an important potential target for the treatment of metabolic diseases (Kajimura et al., 2015). Bioactive compounds in food have attracted much attention as a safe and effective molecular library. It has been reported that garlic is an excellent natural source of bioactive compounds (Gao et al., 2019). In this study, we revealed the beneficial effects of allicin on energy homeostasis in obese mice. Our data show that allicin enhances BAT function, promotes the energy expenditure, inhibits the fat mass accumulation, improves the glucose homeostasis and insulin sensitivity, and alleviates hepatic steatosis. Allicin promotes the activity of sirt1 and induces the downstream PGC1α-Tfam signaling pathway. This is the first study that relatively systematically demonstrates that allicin induces BAT activation and regulates energy homeostasis. Our findings show that administration of allicin using appropriate concentrations may potentially be a therapeutic strategy for obesity and related metabolic syndromes.

Allicin (thio-2-propene-1-sulfinic acid S-allyl ester) is the principal component of garlic and has many physiological functions. Several studies have reported that garlic or its main ingredient, allicin, have anti-oxidation,
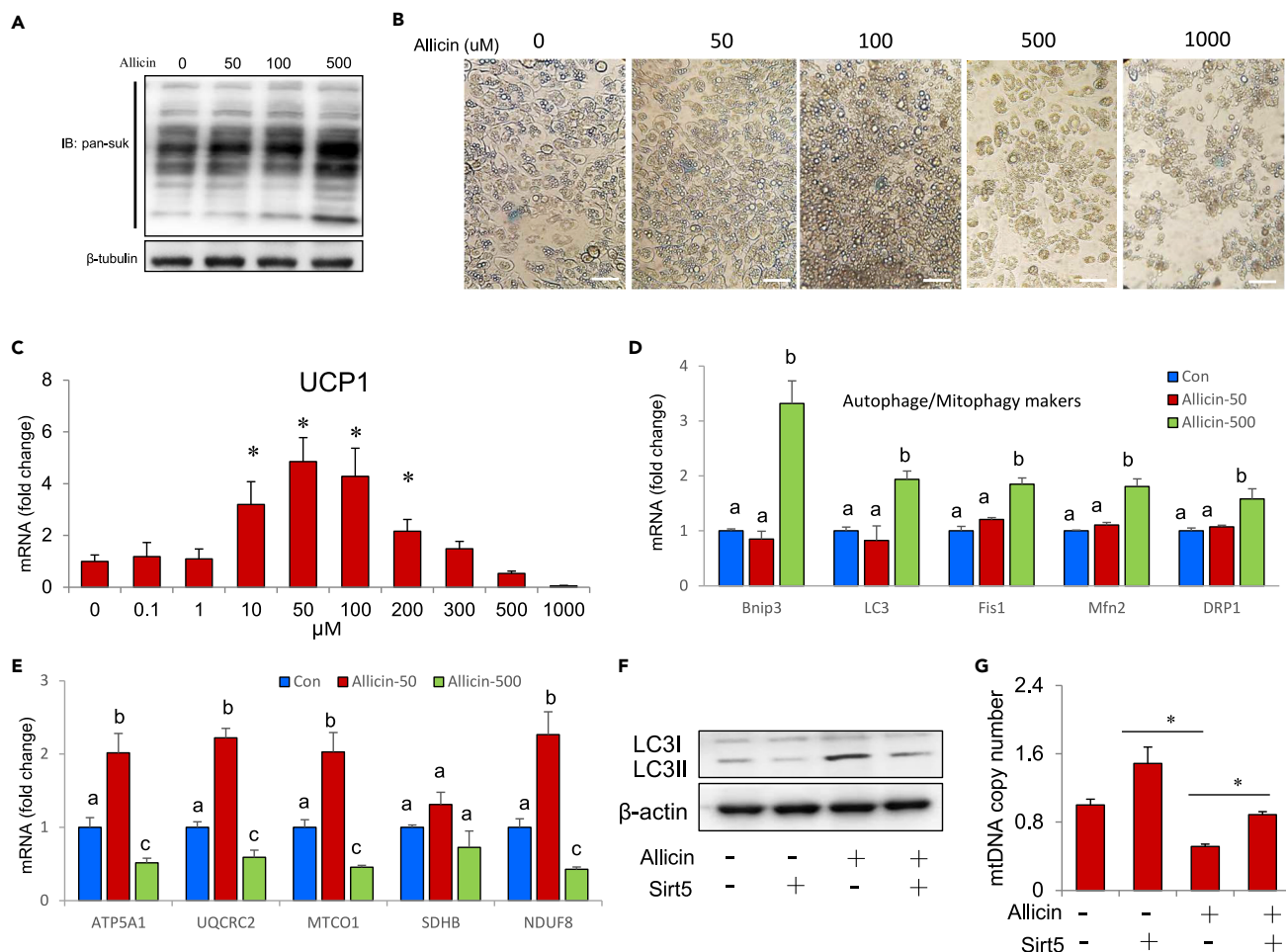
Figure 7. Excessive Amounts of Allicin Induce Mitophagy in Brown Adipocytes

(A) The succinylation levels of general proteins in brown adipocytes with dose-dependent allicin treatment.

(B) The morphology of brown adipocytes treated with different doses of allicin. Scale bars, 50 μm.

(C) mRNA expression levels of UCP1 in brown adipocytes treated with different doses of allicin.

(D) Real-time PCR analysis of autophagy/mitophagy marker genes in brown adipocytes treated with different doses of allicin (0, 50, and 500 μM).

(E) Real-time PCR analysis of mitochondrial Oxphos-related genes in brown adipocytes treated with different doses of allicin (0, 50, and 500 μM).

(F) Overexpression of Sirt5 effectively rescued the high-dose allicin-mediated increase in LC3 in brown adipocytes.

(G) Overexpression of Sirt5 effectively rescues the high-dose allicin-mediated decrease in mitochondrial mtDNA copy number in brown adipocytes. Values represent means ± SEM. Error bars represent SEM; significant differences compared with vehicle controls are indicated by *p < 0.05 (assessed by Student's t test). Different letters indicate signicance among groups (P<0.05).

anti-obesity, anti-hyperinsulinemic, anti-hyperlipidemic, and anti-hypertensive effects (Lee et al., 2019; Elkayam et al., 2003; Hosseini and Hosseinzadeh, 2015). Among these, a research article reported that allicin could induce brown-like adipogenesis and increase lipid oxidation in subcutaneous fat though KLF15 signal cascade (Lee et al., 2019). However, the effect and mechanism of allicin on BAT functions have remained unclear. In addition, research on allicin in relation to regulating energy homeostasis is limited. The present study demonstrated that allicin induces BAT activation, leading to the inhibition of obesity and maintenance of energy homeostasis in mice.

Malfunctions in energy homeostasis, including energy expenditure, food intake, and fat hypertrophy, can cause obesity (Murphy and Bloom, 2006; Farooqi and O'Rahilly, 2005). In the current study, allicin treatment profoundly increased energy expenditure, reduced fat mass, caused body weight gain, and improved the glucose homeostasis in HFD mice. Importantly, a similar effect was further confirmed in Db/Db mice, which is a leptin receptor-deficient genetic obese mice model. This indicates that allicin prevents and alleviates obesity as well as regulates energy metabolism in the body. Furthermore, we investigated the effect of

allicin on BAT activation both in HFD and Db/Db mice and found that allicin treatment more profoundly promotes the activation of BAT in Db/Db mice than in HFD mice (Figures 2 and S4), based on the fact that Db/Db mice are deficient in BAT activity (Trayhurn, 1979). This result indicates that allicin activates BAT and regulates energy metabolism. However, several factors (including thyroid hormones, catecholamine neurotransmission, and cytokines) are secreted by the endocrine system, which can activate brown adipocytes. So, to determine whether the effect of allicin on BAT activation is direct or secondary, *in vitro* allicin treatment of brown adipocytes was performed, which confirmed that allicin could directly activate brown adipocytes.

Information on the effects of allicin on human metabolism is limited, and it is difficult to accurately predict whether the effect of allicin in the human body is similar to that in animals. In our study, we treated human brown adipocytes with allicin and found that it can also dramatically increase the expression levels of UCP1 and related thermogenic genes. This result suggests that allicin may be potentially utilized in regulating energy homeostasis by activating BATs in the human body. Moreover, our findings may serve as reference for future studies on allicin in relation to human metabolic disease. Accumulating evidence has proved that the beiging of WAT is also a critical strategy for the treatment of obesity (Yuan et al., 2017; Shabalina et al., 2013). Consistent with these previous reports, we also found that allicin can induce beige fat formation and markedly increase the expression of beige markers in the subcutaneous fat of HFD mice and Db/Db mice. Importantly, we also further confirmed the beiging induction effect of allicin in human white adipocytes. These results suggest that thermogenic fats, including BAT and beige fat, have a positive regulatory effect on energy homeostasis.

Hepatic steatosis is also a typical phenotype of imbalanced energy homeostasis (You et al., 2017). Nonalcoholic fatty liver (NAFLD) is caused by metabolic syndrome often accompanied by hyperlipidemia, obesity, and related type 2 diabetes (Machado and Cortez-Pinto, 2006). Several studies have reported that garlic and its essential ingredients could protect against NAFLD by regulating lipid metabolism (Lai et al., 2014; Li et al., 2010). Consistently, our data also confirm that allicin could significantly ameliorate lipid accumulation in the liver of HFD and Db/Db mice. In addition, we found that allicin treatment can markedly increase the mRNA expression levels of fatty acid oxidation- and lipolysis-related genes, whereas downregulate the fatty acid synthesis-related and proinflammatory genes. Given the effect of allicin on whole-body energy metabolism by activation of BAT, we hypothesis that the phenotype of improvement of NAFLD in mice is more responsible for the enhanced whole-body energy expenditure and the improved metabolic condition caused by the activation effect of allicin on thermogenic fat. Interestingly, we found that allicin treatment does not significantly inhibit body weight gain under thermoneutral conditions (Figure S5). Simultaneously, allicin treatment did not significantly improve fatty liver after loss of BAT activity (under thermoneutral conditions) in DIO mice (Figure S5G). The above-mentioned results suggest that the anti-obesity role of allicin depends more on the role of BAT activation. However, *in vitro* hepatocyte models require further in-depth analysis.

Allicin is a product obtained from alliin in the presence of alliinase (Elkayam et al., 2003). Recently, we have shown that alliin did not activate BAT and had no significant effect on adiposity or energy metabolism (Zhai et al., 2018). This study confirms that allicin instead of alliin activates brown fat. Allicin and alliin have similar chemical structures; however, their functions significantly vary. Functional differences caused by their molecular structure require further investigation. The identification and allosteric study of the functional groups of allicin may significantly promote the potential utilization of allicin for the treatment of metabolic diseases.

Mitochondria are the main organelles wherein brown fat regulates energy metabolism (Harms and Seale, 2013). In the current study, allicin treatment markedly increased mitochondrial copy number and upregulated OXPHOS proteins in BAT and sWAT in obese mice. In addition, allicin treatment improved the adaptive thermogenic capacity of both HFD and Db/Db mice. PET-CT confirms that allicin treatment enhances glucose uptake and utilization in BAT of obese mice. These results indicate that allicin increases energy metabolism by enhancing mitochondrial function. Recently, it has been reported that adipose tissue-specific sirt1 transgenic mice enhances whole-body energy metabolism and improves insulin resistance (Xu et al., 2013). Phosphorylation of SIRT1 increases its stability, thereby increasing Sirt1 activity (Ford et al., 2008; Nin et al., 2012). PGC1α, a potent regulator of mitochondrial biogenesis, can positively be regulated by SIRT1 (Lagouge et al., 2006). In addition, the activation of SIRT1 can effectively decrease the acetylation
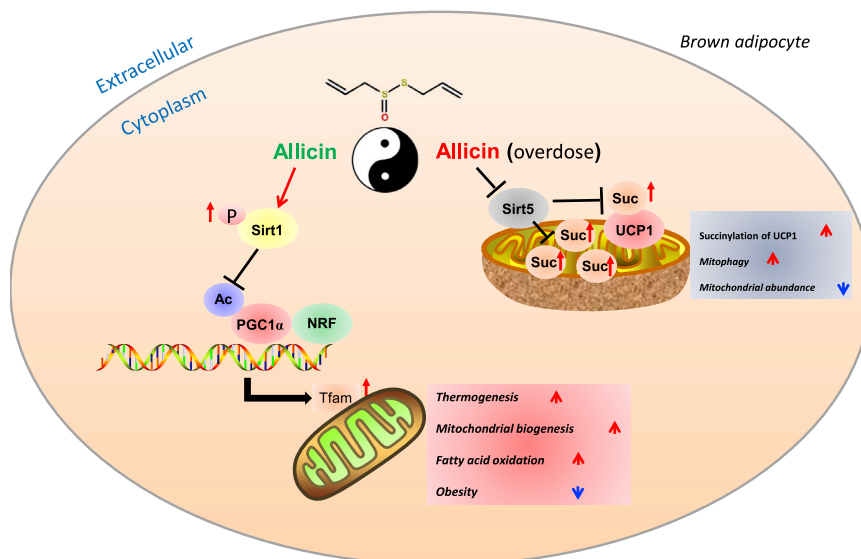
Figure 8. A Proposed Model of the Mechanism by Which Allicin Regulates Mitochondrial Homeostasis in Brown Adipocytes

Allicin promotes the phosphorylation of sirt1 and then activates the PGC1α-Tfam pathway, thereby increasing mitochondrial biogenesis and resulting in increased thermogenesis and fatty acid oxidation. However, allicin treatment at high doses could induce mitophagy due to the increase in succinylation in the mitochondria of brown adipocytes due to the inhibition of sirt5, resulting in mitochondrial dysfunction. These results indicate that allicin plays dual roles, similar to yin and yang properties.

of PGC1α, thereby increasing PGC1α activity (Yuan et al., 2017). Rutin, a small-molecule compound in food, has been demonstrated to enhance BAT function by increasing mitochondrial biogenesis via activation of the Sirt1-PGC1α-Tfam pathway (Yuan et al., 2017). In our study, allicin increased the phosphorylation of SIRT1 protein. Furthermore, our results show that allicin improves SIRT1-mediated PGC1α deacetylation, whereas a deficiency in SIRT1 diminishes allicin-mediated PGC1α deacetylation and offsets the increase in mitochondrial copy number with allicin treatment. In addition, allicin treatment markedly boosted PGC1α and Tfam expression in thermogenic fats from both HFD and Db/Db mice. Collectively, our findings suggest that allicin promotes BAT function partly via the SIRT1-PGC1α-TFAM pathway.

Sirt5, another member of sirtuins, has been reported to regulate several new types of post-transcriptional modifications such as malonylation, succinylation, and glutarylation (Du et al., 2011). Simultaneously, sirt5 can regulate the mitochondrial function though the desuccinylation of proteins in mitochondria (Rardin et al., 2013). Knockout of sirt5 induced the dysfunction of BAT due to the excessive accumulation of succinylation of UCP (Wang et al., 2019). This study is the first to determine that allicin treatment can significantly decrease the expression levels of sirt5 and correspondingly increase the succinylation levels of UCP1 in BAT and brown adipocytes. It is worth noting that the expression level of sirt5 may be affected by the duration of HFD. We also observed that allicin treatment increases the succinylation of UCP1 in a dose-dependent manner; meanwhile the brown adipocytes lost their normal morphology and had UCP1 expression inhibited as the dose increases. Furthermore, excess allicin treatment (500 μM) markedly stimulated autophagy/mitophagy and diminished mitochondrial Oxphos, whereas a moderate allicin concentration (50 μM) upregulated mitochondrial Oxphos-related genes to levels similar to that of autophagy/mitophagy markers (Figures 7D and 7E). Conversely, Sirt5 overexpression partly rescued the above-mentioned phenotypes (Figures 7F and 7G). It indicated that sirt5 is involved in allicin-mediated regulation of mitochondrial homeostasis in brown adipocytes. These findings suggest that excessive or unnecessary allicin treatment disrupts the function of BAT by increasing succinylation levels. These findings suggest that allicin has a dual function. Similar to the yin and yang of the function of things, only moderate applications can play their best function (Figure 8).

Some aspects relating to the mechanism of action of allicin remain unclear, such as how sirt5 regulates mitophagy and induces mitochondrial dysfunction. We screened two candidate proteins (HSP70 and SOD2) that can undergo succinylation modification after allicin treatment in our pull-down sequence result (data

not shown), and their functions may be related to the occurrence of autophagy. SOD2 can regulate autophagy via mitochondrial reactive oxygen species (ROS) (Liu et al., 2019). Interestingly, a recent study has shown that Hsp70 modulates SOD2 activity by promoting the import of SOD2 into mitochondria, which indicates that Hsp70 has a physiological mechanism that is essential for the regulation of mitochondrial redox balance (Zemanovic et al., 2018). Thus, HSP70 and SOD2 may undergo overmuch succinylation modification after allicin treatment at excessively high concentrations, which may impair their regulation of mitochondrial ROS and in turn induce autophagy/mitophagy. However, we also hypothesize that the inhibition of sirt5 may cause extensive succinylation of mitochondrial proteins, which in turn disrupt mitochondrial function and induce mitophagy, including synergy of various mitochondrial proteins. So, this phenotype should not be controlled by a single or couple proteins but may partly contribute to this phenotype.

In summary, the present study demonstrated that allicin regulates energy homeostasis by promoting BAT activation partly via the SIRT1-PGC1α-TFAM pathway. Our findings also provide evidence suggesting that allicin promotes succinylation by inhibiting sirt5, and that allicin treatment at excessively high concentrations disrupts mitochondrial homeostasis. Thus, we propose the concept of yin and yang for allicin function. In general, the application of allicin at a moderate concentration may be potentially used as a novel strategy for the prevention and/or treatment of obesity and related metabolic disorders.

METHODS

All methods can be found in the accompanying Transparent Methods supplemental file.

Limitations of the Study

In this study, the mechanism by which allicin downregulates Sirt5 is unclear. It may be a direct or indirect regulation, such as allicin-induced DNA or RNA changes in the level of epigenetic modification, which needs to be further studied in the future. Besides, a recent report showed that allicin induces browning in WAT via KLF15 signaling (Lee et al., 2019). In our study, we did not investigate the contribution of KLF15 signaling in BAT, even though this is an interesting point. Notably, our research does not rule out other alternative mechanisms of the anti-obesity effects of allicin, such as increased energy expenditure via improvement of gut microbiota, reduced adipocyte hypertrophy via modulation of angiogenesis, induced activation of BAT via KLF15 signaling, and reduced adipogenesis and inflammation. Moreover, the concentration of allicin may be confusing or unnecessary to reach 500 μm *in vivo*, whereas *in vitro* studies are difficult to directly link to *in vivo* studies. At least our study hints that allicin has the possibility of disturbing mitochondrial function through regulation of succinylation. So, the stimulation of Allicin *in vivo* or at the tissue level needs to be further studied.

Resource Availability

Lead Contact

Kunlun Huang (hkl009@163.com).

Materials Availability

This study did not generate new unique reagents.

Data and Code Availability

There is no available unpublished custom code, software, or algorithm.

SUPPLEMENTAL INFORMATION

Supplemental Information can be found online at https://doi.org/10.1016/j.isci.2020.101113.

AUTHOR CONTRIBUTIONS

K.H., Y.L., and C.Z. conceived and supervised the study, designed the experiments, and wrote the paper. C.Z. and Y.S. designed and/or performed most of the experiments, interpreted the results, generated the

figures and tables, and wrote the paper. X.H. and Y.S. participated in designing the experiments and reviewed the paper. All other authors performed experiments and/or discussed the results and reviewed the paper.

DECLARATION OF INTERESTS

The authors declare that they have no conflict of interest.

REFERENCES

Altshuler-Keylin, S., and Kajimura, S. (2017). Mitochondrial homeostasis in adipose tissue remodeling. Sci. Signal. *10*, https://doi.org/10.1126/scisignal.aai9248.

Boström, P., Wu, J., Jedrychowski, M.P., Korde, A., Ye, L., Lo, J.C., Rasbach, K.A., Boström, E.A., Choi, J.H., Long, J.Z., et al. (2012). A PGC1-alpha-dependent myokine that drives brown-fat-like development of white fat and thermogenesis. Nature *481*, 463–468.

Boutant, M., Joffraud, M., Kulkarni, S.S., García-Casarrubios, E., García-Roves, P.M., Ratajczak, J., Fernández-Marcos, P.J., Valverde, A.M., Serrano, M., and Cantó, C. (2015). SIRT1 enhances glucose tolerance by potentiating brown adipose tissue function. Mol. Metab. *4*, 118–131.

Cannon, B., and Nedergaard, J. (2004). Brown adipose tissue: function and physiological significance. Physiol. Rev. *84*, 277–359.

Chalkiadaki, A., and Guarente, L. (2012). High-fat diet triggers inflammation-induced cleavage of SIRT1 in adipose tissue to promote metabolic dysfunction. Cell Metab. *16*, 180–188.

Chan, J.Y., Yuen, A.C., Chan, R.Y., and Chan, S.W. (2013). A review of the cardiovascular benefits and antioxidant properties of allicin. Phytother. Res. *27*, 637–646.

Chi, Q.S., and Wang, D.H. (2011). Thermal physiology and energetics in male desert hamsters (Phodopus roborovskii) during cold acclimation. J. Comp. Physiol. B *181*, 91–103.

Ding, G., Zhao, J., and Jiang, D. (2016). Allicin inhibits oxidative stress-induced mitochondrial dysfunction and apoptosis by promoting PI3K/AKT and CREB/ERK signaling in osteoblast cells. Exp. Ther. Med. *11*, 2553–2560.

Du, J., Zhou, Y., Su, X., Yu, J.J., Khan, S., Jiang, H., Kim, J., Woo, J., Kim, J.H., Choi, B.H., et al. (2011). Sirt5 is a NAD-dependent protein lysine demalonylase and desuccinylase. Science *334*, 806–809.

Elkayam, A., Mirelman, D., Peleg, E., Wilchek, M., Miron, T., Rabinkov, A., Oron-Herman, M., and Rosenthal, T. (2003). The effects of allicin on weight in fructose-induced hyperinsulinemic, hyperlipidemic, hypertensive rats. Am. J. Hypertens. *16*, 1053–1056.

El-Sheakh, A.R., Ghoneim, H.A., Suddek, G.M., and Ammar, E.S.M. (2016). Attenuation of oxidative stress, inflammation, and endothelial dysfunction in hypercholesterolemic rabbits by allicin. Can. J. Physiol. Pharmacol. *94*, 216–224.

Farooqi, I.S., and O'Rahilly, S. (2005). Monogenic obesity in humans. Annu. Rev. Med. *56*, 443–458.

Ford, J., Ahmed, S., Allison, S., Jiang, M., and Milner, J. (2008). JNK2-dependent regulation of SIRT1 protein stability. Cell Cycle *7*, 3091–3097.

Frye, R.A. (2000). Phylogenetic classification of prokaryotic and eukaryotic Sir2-like proteins. Biochem. Biophys. Res. Commun. *273*, 793–798.

Gao, W., Wang, W., Zhang, J., Deng, P., Hu, J., Yang, J., and Deng, Z. (2019). Allicin ameliorates obesity comorbid depressive-like behaviors: involvement of the oxidative stress, mitochondrial function, autophagy, insulin resistance and NOX/Nrf2 imbalance in mice. Metab. Brain Dis. *34*, 1267–1280.

Geserick, M., Vogel, M., Gausche, R., Lipek, T., Spielau, U., Keller, E., Pfäffle, R., Kiess, W., and Körner, A. (2018). Acceleration of BMI in early childhood and risk of sustained obesity. N. Engl. J. Med. *379*, 1303–1312.

Harms, M., and Seale, P. (2013). Brown and beige fat: development, function and therapeutic potential. Nat. Med. *19*, 1252–1263.

Hosseini, A., and Hosseinzadeh, H. (2015). A review on the effects of Allium sativum (Garlic) in metabolic syndrome. J. Endocrinol. Invest. *38*, 1147–1157.

Kajimura, S., Spiegelman, B.M., and Seale, P. (2015). Brown and beige fat: physiological roles beyond heat generation. Cell Metab. *22*, 546–559.

Lagouge, M., Argmann, C., Gerhart-Hines, Z., Meziane, H., Lerin, C., Daussin, F., Messadeq, N., Milne, J., Lambert, P., Elliott, P., et al. (2006). Resveratrol improves mitochondrial function and protects against metabolic disease by activating SIRT1 and PGC-1alpha. Cell *127*, 1109–1122.

Lai, Y.S., Chen, W.C., Ho, C.T., Lu, K.H., Lin, S.H., Tseng, H.C., Lin, S.Y., and Sheen, L.Y. (2014). Garlic essential oil protects against obesity-triggered nonalcoholic fatty liver disease through modulation of lipid metabolism and oxidative stress. J. Agric. Food Chem. *62*, 5897–5906.

Landry, J., Sutton, A., Tafrov, S.T., Heller, R.C., Stebbins, J., Pillus, L., and Sternglanz, R. (2000). The silencing protein SIR2 and its homologs are NAD-dependent protein deacetylases. Proc. Natl. Acad. Sci. U S A *97*, 5807–5811.

Lee, C.G., Rhee, D.K., Kim, B.O., Um, S.H., and Pyo, S. (2019). Allicin induces beige-like adipocytes via KLF15 signal cascade. J. Nutr. Biochem. *64*, 13–24.

Li, W., Wang, D., Song, G., Zuo, C., Qiao, X., and Qin, S. (2010). The effect of combination therapy of allicin and fenofibrate on high fat diet-induced vascular endothelium dysfunction and liver damage in rats. Lipids Health Dis. *9*, 131.

Li, X., Qi, J., Zhu, Q., He, Y., Wang, Y., Lu, Y., Wu, H., and Sun, Y. (2019). The role of androgen in autophagy of granulosa cells from PCOS. Gynecol. Endocrinol. *35*, 669–672.

Liesa, M., and Shirihai, O.S. (2013). Mitochondrial dynamics in the regulation of nutrient utilization and energy expenditure. Cell Metab. *17*, 491–506.

Liu, T., Ma, X., Ouyang, T., Chen, H., Xiao, Y., Huang, Y., Liu, J., and Xu, M. (2019). Efficacy of 5-aminolevulinic acid-based photodynamic therapy against keloid compromised by downregulation of SIRT1-SIRT3-SOD2-mROS dependent autophagy pathway. Redox Biol. *20*, 195–203.

Machado, M., and Cortez-Pinto, H. (2006). Non-alcoholic steatohepatitis and metabolic syndrome. Curr. Opin. Clin. Nutr. Metab. Care *9*, 637–642.

Matsushita, M., Yoneshiro, T., Aita, S., Kameya, T., Sugie, H., and Saito, M. (2014). Impact of brown adipose tissue on body fatness and glucose metabolism in healthy humans. Int. J. Obes. (Lond) *38*, 812–817.

McRae, M.P. (2005). A review of studies of garlic (Allium sativum) on serum lipids and blood pressure before and after 1994: does the amount of allicin released from garlic powder tablets play a role? J. Chiropr. Med. *4*, 182–190.

Merrick, D., Sakers, A., Irgebay, Z., Okada, C., Calvert, C., Morley, M.P., Percec, I., and Seale, P. (2019). Identification of a mesenchymal progenitor cell hierarchy in adipose tissue. Science *364*, https://doi.org/10.1126/science.aav2501.

Murphy, K.G., and Bloom, S.R. (2006). Gut hormones and the regulation of energy homeostasis. Nature *444*, 854–859.

Nin, V., Escande, C., Chini, C.C., Giri, S., Camacho-Pereira, J., Matalonga, J., Lou, Z., and Chini, E.N. (2012). Role of deleted in breast cancer 1 (DBC1) protein in SIRT1 deacetylase activation induced by protein kinase A and AMP-activated protein kinase. J. Biol. Chem. *287*, 23489–23501.

Nishtar, S., Gluckman, P., and Armstrong, T. (2016). Ending childhood obesity: a time for action. Lancet *387*, 825–827.

Peirce, V., Carobbio, S., and Vidal-Puig, A. (2014). The different shades of fat. Nature *510*, 76–83.

Rardin, M.J., He, W., Nishida, Y., Newman, J.C., Carrico, C., Danielson, S.R., Guo, A., Gut, P., Sahu, A.K., Li, B., et al. (2013). SIRT5 regulates the mitochondrial lysine succinylome and metabolic networks. Cell Metab. *18*, 920–933.

Ro, S.H., Jang, Y., Bae, J., Kim, I.M., Schaecher, C., and Shomo, Z.D. (2019). Autophagy in adipocyte browning: emerging drug target for intervention in obesity. Front. Physiol. *10*, 22.

Seale, P., Conroe, H.M., Estall, J., Kajimura, S., Frontini, A., Ishibashi, J., Cohen, P., Cinti, S., and Spiegelman, B.M. (2011). Prdm16 determines the thermogenic program of subcutaneous white adipose tissue in mice. J. Clin. Invest. *121*, 96–105.

Shabalina, I.G., Petrovic, N., de Jong, J.M., Kalinovich, A.V., Cannon, B., and Nedergaard, J. (2013). UCP1 in brite/beige adipose tissue

mitochondria is functionally thermogenic. Cell Rep. *5*, 1196–1203.

Shuai, L., Zhang, L.N., Li, B.H., Tang, C.L., Wu, L.Y., Li, J., and Li, J.Y. (2019). SIRT5 regulates Brown adipocyte differentiation and browning of subcutaneous white adipose tissue. Diabetes *68*, 1449–1461.

Trayhurn, P. (1979). Thermoregulation in the diabetic-obese (Db/Db) mouse. The role of non-shivering thermogenesis in energy balance. Pflugers Arch. *380*, 227–232.

Wang, G., Meyer, J.G., Cai, W., Softic, S., Li, M.E., Verdin, E., Newgard, C., Schilling, B., and Kahn, C.R. (2019). Regulation of UCP1 and mitochondrial metabolism in brown adipose tissue by reversible succinylation. Mol. Cell *74*, 844–857.e7.

Wu, J., Boström, P., Sparks, L.M., Ye, L., Choi, J.H., Giang, A.H., Khandekar, M., Virtanen, K.A., Nuutila, P., Schaart, G., et al. (2012). Beige adipocytes are a distinct type of thermogenic fat cell in mouse and human. Cell *150*, 366–376.

Xu, C., Bai, B., Fan, P., Cai, Y., Huang, B., Law, I.K., Liu, L., Xu, A., Tung, C., Li, X., et al. (2013). Selective overexpression of human SIRT1 in adipose tissue enhances energy homeostasis and prevents the deterioration of insulin sensitivity with ageing in mice. Am. J. Transl. Res. *5*, 412–426.

Yin, N., Zhang, H., Ye, R., Dong, M., Lin, J., Zhou, H., Huang, Y., Chen, L., Jiang, X., Nagaoka, K., et al. (2019). Fluvastatin sodium ameliorates obesity through Brown fat activation. Int. J. Mol. Sci. *20*, https://doi.org/10.3390/ijms20071622.

You, Y., Yuan, X., Liu, X., Liang, C., Meng, M., Huang, Y., Han, X., Guo, J., Guo, Y., Ren, C., et al. (2017). Cyanidin-3-glucoside increases whole body energy metabolism by upregulating brown adipose tissue mitochondrial function. Mol. Nutr. Food Res. *61*, https://doi.org/10.1002/mnfr.201700261.

Yuan, X., Wei, G., You, Y., Huang, Y., Lee, H.J., Dong, M., Lin, J., Hu, T., Zhang, H., Zhang, C., et al. (2017). Rutin ameliorates obesity through brown fat activation. FASEB J. *31*, 333–345.

Zemanovic, S., Ivanov, M.V., Ivanova, L.V., Bhatnagar, A., Michalkiewicz, T., Teng, R.J., Kumar, S., Rathore, R., Pritchard, K.A., Jr., Konduri, G.G., and Afolayan, A.J. (2018). Dynamic phosphorylation of the C terminus of Hsp70 regulates the mitochondrial import of SOD2 and redox balance. Cell Rep. *25*, 2605–2616.e7.

Zhai, B., Zhang, C., Sheng, Y., Zhao, C., He, X., Xu, W., Huang, K., and Luo, Y. (2018). Hypoglycemic and hypolipidemic effect of S-allyl-cysteine sulfoxide (alliin) in DIO mice. Sci. Rep. *8*, 3527.

Zhang, C., Wang, J., Zhang, H., Liu, S., Lee, H.J., Jin, W., and Cheng, J. (2018). Hepatitis C virus core protein induces hepatic steatosis via Sirt1-dependent pathway. Liver Int. *38*, 803–812.

Zhang, C., Weng, Y., Shi, F., and Jin, W. (2016). The engrailed-1 gene stimulates Brown adipogenesis. Stem Cell Int. *2016*, 7369491.

Zhou, J., Wu, N.N., Yin, R.L., Ma, W., Yan, C., Feng, Y.M., Zhang, C.H., and Zhao, D. (2018). Activation of brown adipocytes by placental growth factor. Biochem. Biophys. Res. Commun. *504*, 470–477.

Supplemental Information

Allicin Regulates Energy Homeostasis

through Brown Adipose Tissue

Chuanhai Zhang, Xiaoyun He, Yao Sheng, Jia Xu, Cui Yang, Shujuan Zheng, Junyu Liu, Haoyu Li, Jianbing Ge, Minglan Yang, Baiqiang Zhai, Wentao Xu, Yunbo Luo, and Kunlun Huang

Supplemental Information

This section includes:

Figures S1 to S9

Tables S1

Transparent methods

References for supplemental information
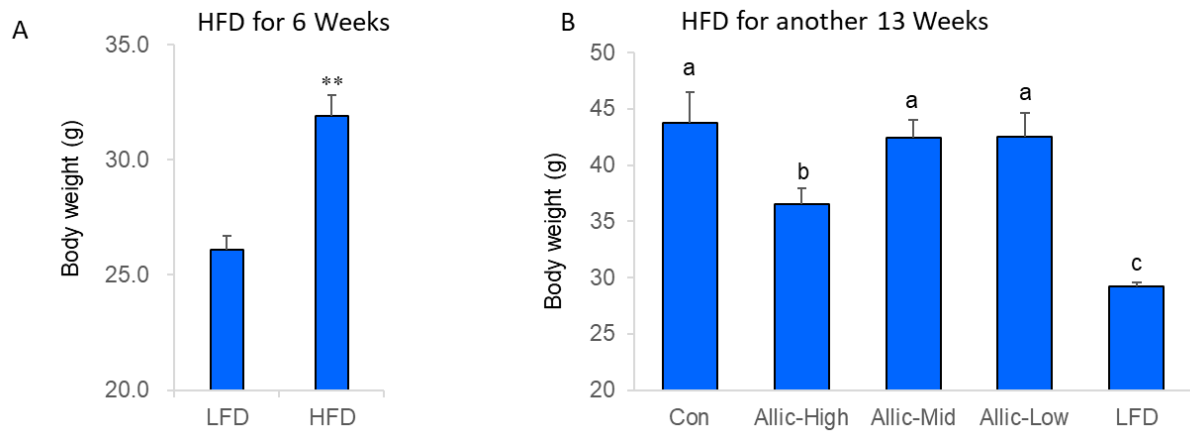
Supplementary figure legends

Figure s1. Related to Figure 1. (A) The body weight of mice fed with chow or high-fat diet for the first six weeks before allicin treatment. (B) The body weight of different groups of mice fed on chow or high-fat diet for 13 weeks. Values represent the means ± SEM. Error bars represent SEM; significant differences compared to vehicle controls are indicated by **p < 0.01 (assessed by student's *t*-test). Different letters indicate significance among groups (P<0.05).
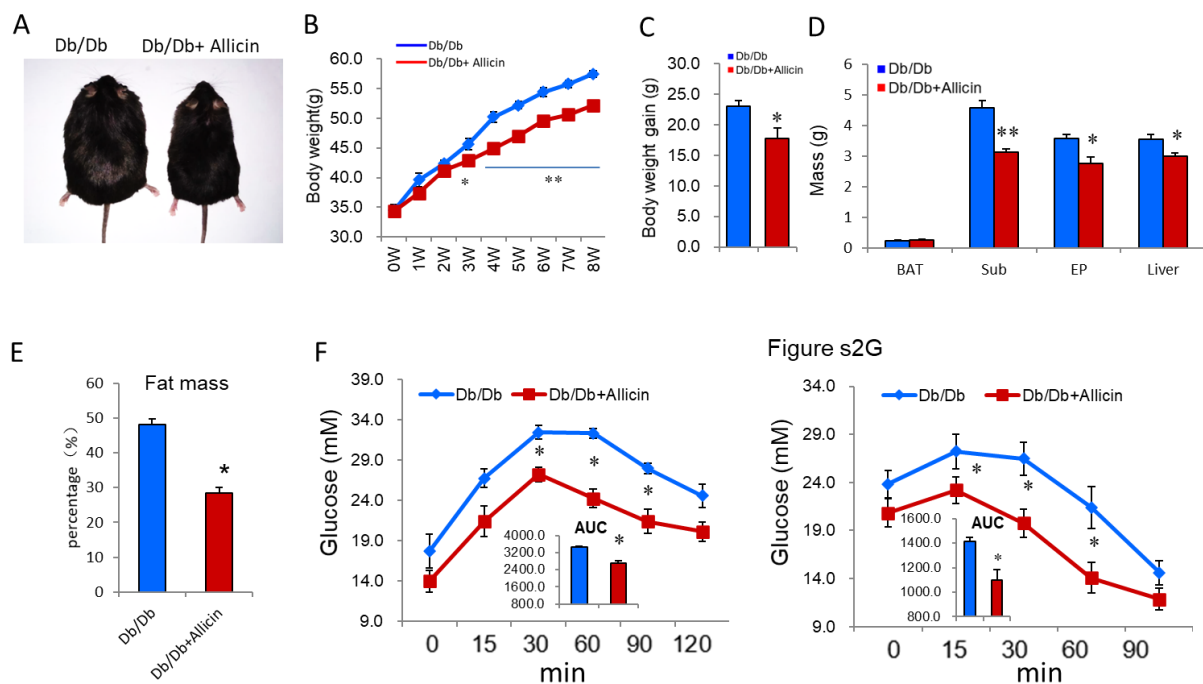
Figure s2. Related to Figure 1. Allicin reduces body weight gain and improves glucose homeostasis in leptin-receptor deficiency mice (Db/Db mice).

(A) Body-shape image of Db/Db control mice and mice treated with allicin. (B) Body weight of Db/Db mice treated with vehicle or allicin. (n=5). (C) Body weight gain of Db/Db control mice and mice treated with allicin. (n=5). (D) Organ weight of control and allicin-treated Db/Db mice (n = 5). (E) Body fat percentage test using NMR. (F) Glucose tolerance test of control and allicin-treated Db/Db mice (I.P. with glucose as 0.5 g/kg after 16 h of fasting) (n=5). The average area under the curve (n = 5). (G) Insulin tolerance test was performed on control and allicin-treated Db/Db mice (injection insulin with 1.0 U/kg after 6 h of fasting (n = 5). The average area under the curve (n=5). Values represent means ± SEM. Error bars represent SEM; significant differences compared to vehicle controls are indicated by *p < 0.05, **p < 0.01 (assessed by student's *t*-test).
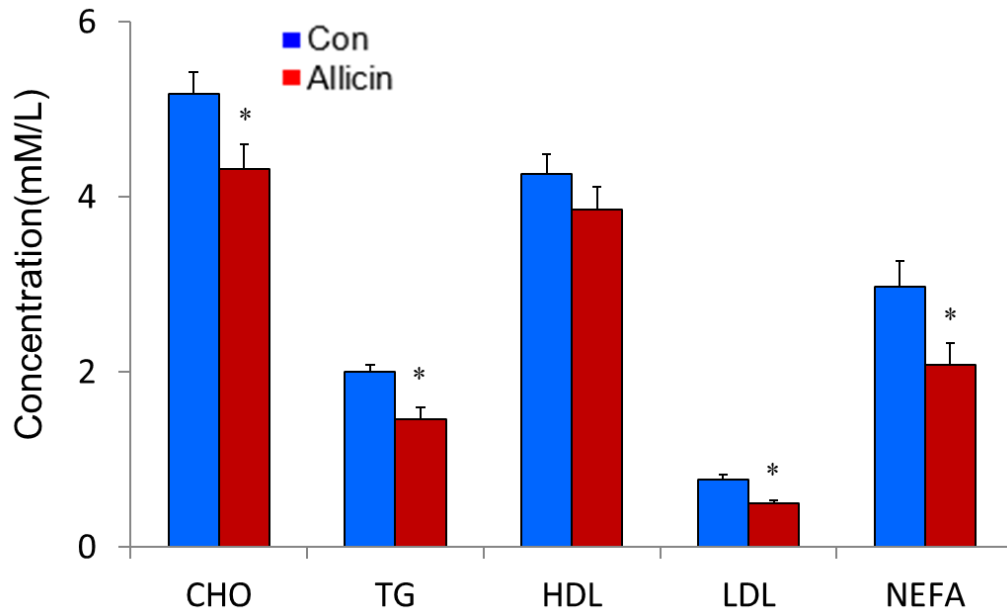
Figure S3. Related to Figure 1 and Figure 4. Serum lipid profiles of control and allicin-treated DIO mice. Values represent the means ± SEM. Error bars represent SEM; significant differences compared to vehicle controls are indicated by *p < 0.05 (assessed by student's *t*-test).
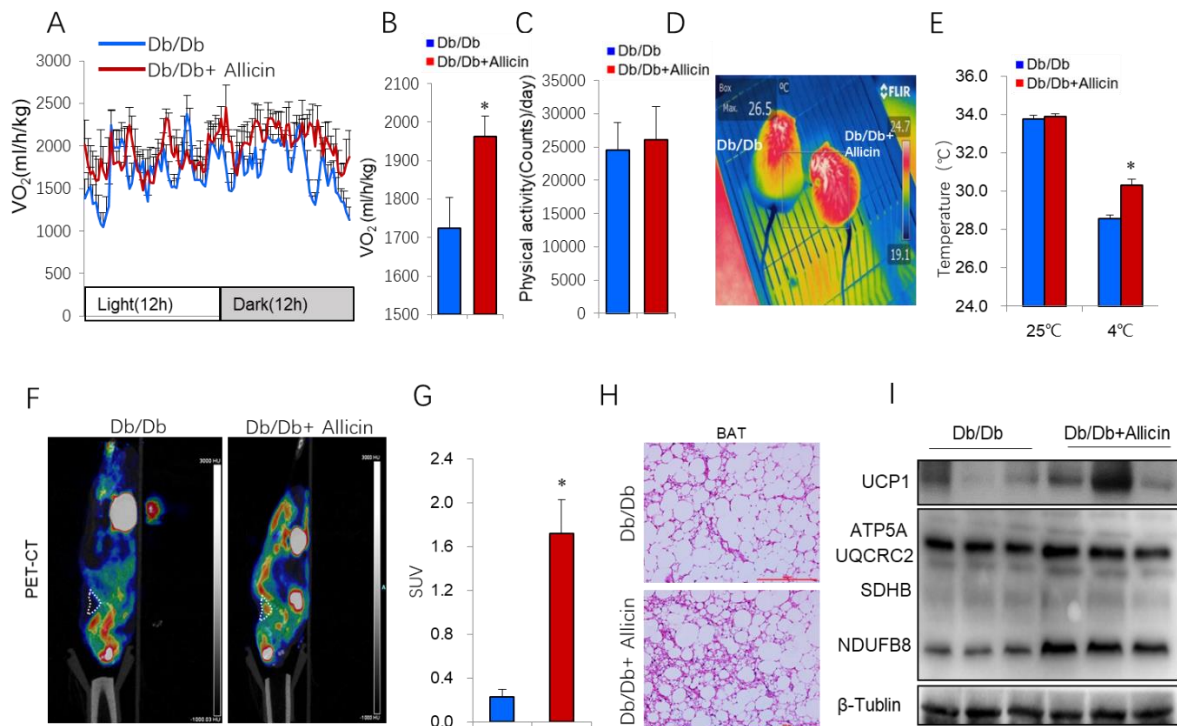
Figure s4. Related to Figure 2. Allicin increases energy expenditure and enhances BAT activity in leptin-receptor deficiency mice (Db/Db mice).

(A and B) Energy expenditure was assessed by oxygen consumption (VO2) in Db/Db mice after eight weeks of allicin treatment (B) (n = 5); (D) Infrared thermal images of control and allicin-treated Db/Db mice, which showed more thermal signals in the interscapular BAT position. (E) The core body temperature of control and allicin-treated mice at room temperature (25°C) and after cold stimulation (4°C for 4 h). (F-G) PET/CT images after injection of 18F-FDG into Db/Db mice treated with vehicle and allicin for eight weeks. White triangles indicate the anatomical site of the interscapular BAT (n=3). Mean standard uptake value (SUV) of 18F-FDG in BAT (F). (H) H&E staining of BAT form control and allicin-treated Db/Db mice. Scale bars, 200μm. (I) UCP1 and OXPHOS expression levels in BAT from control and allicin-treated Db/Db mice. Values represent the means ± SEM. Error bars represent SEM; significant differences compared to vehicle controls are indicated by *p < 0.05 (assessed by student's *t*-test).
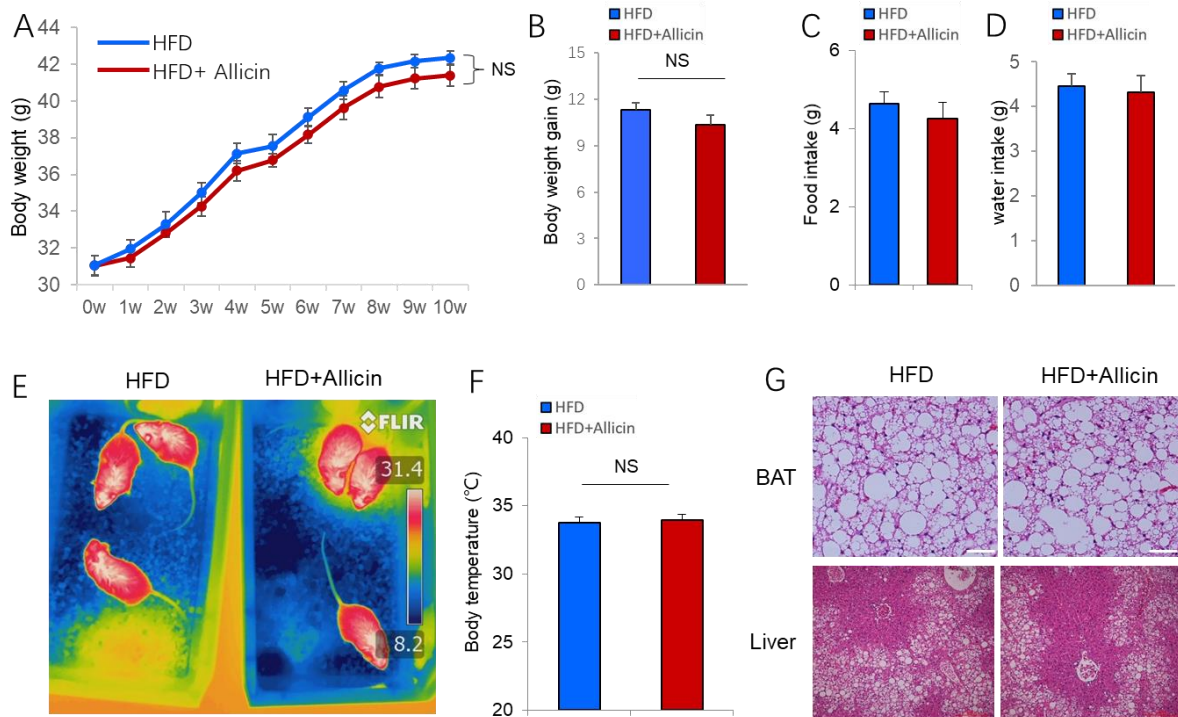
Figure S5. Related to Figure 2. Allicin treatment does not alleviate obesity under thermoneutral conditions.

(A) Body weight and body weight gain (B) in HFD mice treated with/without allicin under thermoneutral conditions (28°C–30°C). (C and D) Food and water intake. (E) Infrared thermal images of control and allicin-treated Db/Db mice. (F) Rectal temperature of the mice. (G) H&E staining of BAT and liver of HFD mice treated with/without allicin. Scale bars, 100μm. Values represent the means ± SEM. Error bars represent SEM;
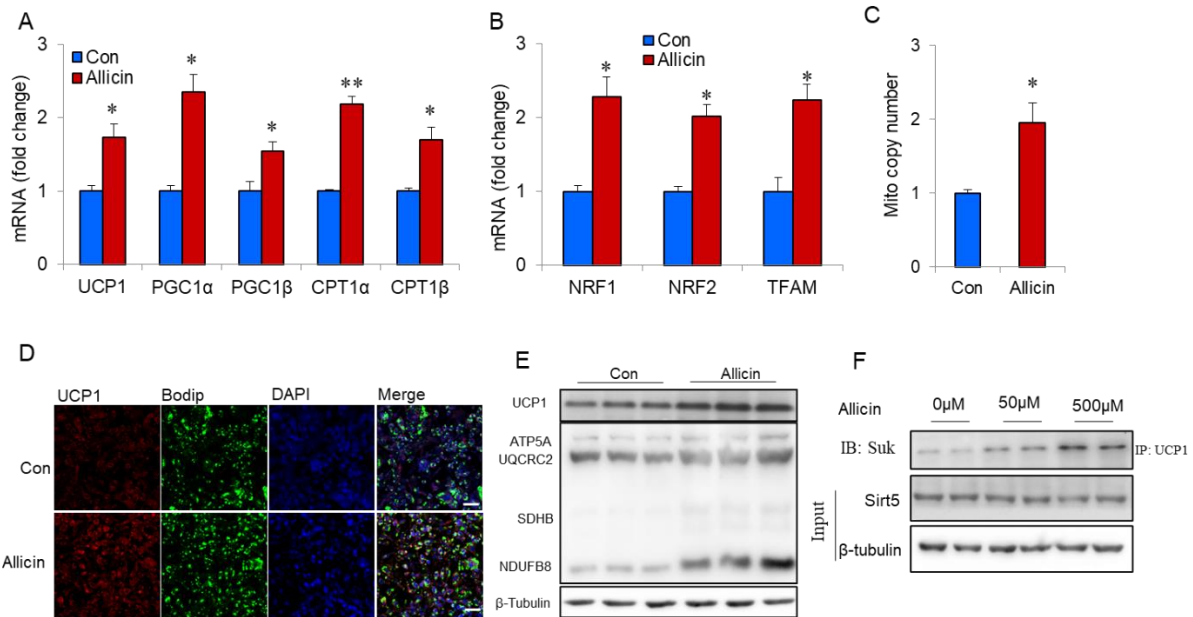
Figure S6. Related to Figure 3 and Figure 6. Allicin increases the activity of human brown adipocytes.

(A) Thermogenic gene expression in human brown adipocytes treated with 50 μM allicin or DMSO. (B) mRNA expression levels of the mitochondrial biogenesis-related genes in human brown adipocytes treated with allicin or DMSO. (C) Mitochondrial mtDNA copy number in human brown adipocytes treated with allicin or DMSO. (D) Immunofluorescence staining of UCP1 and BODIPY in human brown adipocytes treated with allicin or DMSO on day 6 of brown adipogenesis. Scale bars, 50μm. (E) Protein expression levels of UCP1 and OXPHOS in human brown adipocytes treated with DMSO or allicin. Values represent means ± SEM. Error bars represent SEM; significant differences compared to vehicle controls are indicated by $*p < 0.05$, $**p < 0.01$ (assessed by student's t-test).
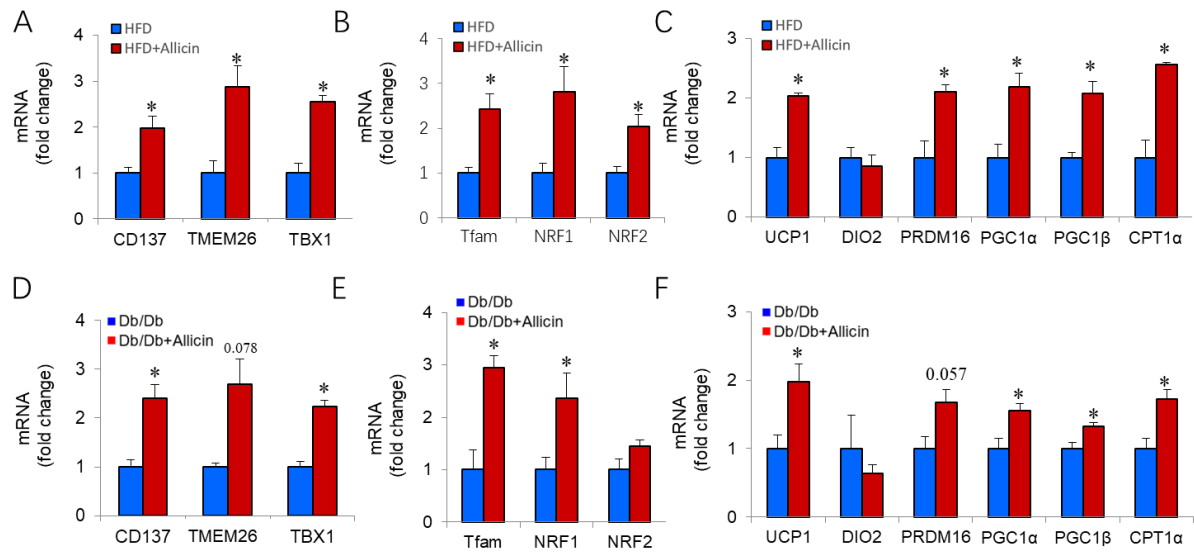
Figure S7. Related to Figure 1-3. Allicin induces beiging in subcutaneous fat in obese mice.

(A-C) Results of real-time PCR analysis of beige cell specific marker genes (A), mitochondrial biogenesis genes (B), and thermogenic-related genes (C) in sWAT from DIO mice treated with and/or without allicin. (n = 3). (D-F) Results of real-time PCR analysis of beige cell-specific marker genes (D), mitochondrial biogenesis genes (E), and thermogenic-related genes (F) in sWAT from DB/DB mice treated with and/or without allicin. (n = 3). (G) mtDNA copy number of sWAT from control and allicin-treated DIO mice and DB/DB mice (I) (n = 3). (H and J) Relative protein levels of UCP1 and OXPHOS in sWAT from control and allicin-treated DIO mice (H) and DB/DB mice (J). Values represent means ± SEM. Error bars represent SEM; significant differences compared to vehicle controls are indicated by *p < 0.05 (assessed by student's *t*-test).
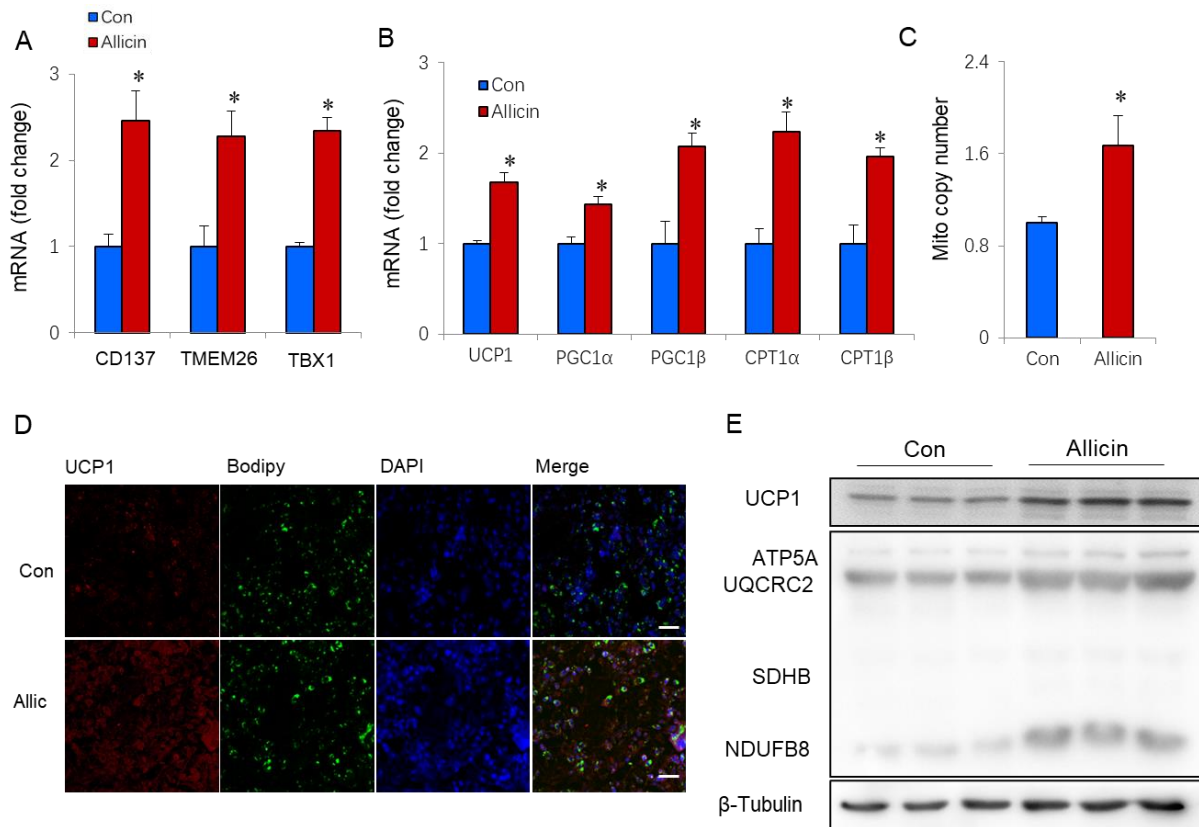
Figure S8. Related to Figure 1-3. Allicin induces beiging in human white adipocytes.

(A) mRNA expression levels of the beige marker genes in human white adipocytes treated with allicin or DMSO. (B) Thermogenic gene expression in human white adipocytes treated with 50 µM allicin or DMSO. (C) Mitochondrial mtDNA copy number in human white adipocytes treated with allicin or DMSO. (D) Immunofluorescence staining of UCP1 and BODIPY in human white adipocytes treated with allicin or DMSO on day 6 of brown adipogenesis. Scale bars, 50µm. (E) The protein levels of UCP1 and OXPHOS in human white adipocytes treated with DMSO or allicin. Values represent the means ± SEM. Error bars represent SEM; significant differences compared to vehicle controls are indicated by *$p < 0.05$ (assessed by student's t-test).

Table S1. Primers used for real-time PCR analysis. Related to Figure 2–7 and FigureS6-S8.

Gene	Forward primer (5' → 3')	Reverse primer (5' → 3')
Human-Cyclophilin	TAAAGCATACGGGTCCTGGC	GACTGAGTGGTTGGATGGCA
Human-UCP1	GCAGGGAAAGAAACAGCACC	CCCGTGTAGCGAGGTTTGAT
Human-PGC1α	CAGGCAGTAGATCCTCTTCAAG	TCCTCGTAGCTGTCATACCTG
Human-PGC1β	GCCCAGATACACTGACTACG	CTCGAGGGTTAAGGCTGTTATC
Human-NRF1	GAGGCGCTGGAATGAACAAG	AGGAACACAGCAAACACCCT
Human-NRF2	TCAGCGACGGAAAGAGTATGA	CCACTGGTTTCTGACTGGATGT
Human-Tfam	CCATATTTAAAGCTCAGAACCCAG	CTCCGCCCTATAAGCATCTTG
Human-CPT1β	ATCCTACTCCTATGACCCCG	TCTGCATTGAGACCCAACTG
Human-CPT1α	CCTCCAGTTGGCTTATCGTG	TTCTTCGTCTGGCTGGACAT
Human-CD137	AGCTGTTACAACATAGTAGCCAC	TCCTGCAATGATCTTGTCCTCT
Human-TBX1	ACGACAACGGCCACATTATTC	CCTCGGCATATTTCTCGCTATCT
Human-TMEM26	ATGGAGGGACTGGTCTTCCTT	CTTCACCTCGGTCACTCGC
Mouse-Cyclophilin	CAAATGCTGGACCAAACACAA	GCCATCCAGCCATTCAGTCT
Mouse-Ucp1	GGCAAAAACAGAAGGATTGC	TAAGCCGGCTGAGATCTTGT
Mouse-Prdm16	GAAGTCACAGGAGGACACGG	CTCGCTCCTCAACACACCTC
Mouse-Cpt1α	GACTCCGCTCGCTCATTCC	GACTGTGAACTGGAAGGCCA
Mouse-Mcad	ACTCGAAAGCGGCTCACAA	ACGGGGATAATCTCCTCTCTGG
Mouse-Pgc1α	ACAGCTTTCTGGGTGGATTG	TGAGGACCGCTAGCAAGTTT
Mouse-Pgc1β	CGTATTTGAGGACAGCAGCA	TACTGGGTGGGCTCTGGTAG
Mouse-Pparα	AGCCTCAGCCAAGTTGAAGT	TGGGGAGAGAGGACAGATGG
Mouse-Tbx1	GGCAGGCAGACGAATGTTC	TTGTCATCTACGGGCACAAAG
Mouse-Tmem26	ACCCTGTCATCCCACAGAG	TGTTTGGTGGAGTCCTAAGGTC
Mouse-Cd137	CGTGCAGAACTCCTGTGATAAC	GTCCACCTATGCTGGAGAAGG
Mouse-SIRT1	GCCAGAGTCCAAGTTTAGAAGA	CCATCAGTCCCAAATCCAG
Mouse-ACC	GCTGCTCGGATCACTAGTGAA	TTCTGCTATCAGTCTGTCCAG
Mouse-FASN	GCTGCTCGGATCACTAGTGAA	TGTAGCCCACGAGTGTCTCG
Mouse-SREBP1	GGAGGGGTAGGGCCAACGGCCT	CATGTCTTCGAAAGTGCAATCC
Mouse-HSL	CTGAGATTGAGGTGCTGTCG	CAAGGGAGGTGAGATGGTAAC
Mouse-Atgl	GCGCCAGGACTGGAAAGAAT	TGAGAACGCTGAGGCTTTGAT
Mouse-IL6	AGACAAAGCCAGAGTCCTTCAG	GCCACTCCTTCTGTGACTCCAG
Mouse-IL1β	TTCAGGCAGGCAGTATCACTC	GAAGGTCCACGGGAAAGACAC
Mouse-Tfam	TGGGCCTCTCATGCACCACC	GAGGCAACCTGACCACTCTCCCT
Mouse-Nrf1	CAACAGGGAAGAAACGGAAA	GCACCACATTCTCCAAAGGT
Mouse-Nrf2	CCCCCGAGGACACTTCTTATG	AGCAGCCAGATGGGCAGTTA
Mouse-ATP5A1	TTTGCCCAGTTTGGTTCTGAT	CCCGTACACCCGCATAGATAA
Mouse-UQCRC2	TGGCTCTGGTTGGACTTGGT	TTTCACCTCCACGGTATTTGG
Mouse-MITO1	ACACATGAGCAAAAGCCCAC	AGTCTGAGTAGCGTCGTGGT
Mouse-SDHB	CTGTCGAGGGGCACAGAC	CAACACCATAGGTCCGCACT
Mouse-NDUFB8	GGCACGTGTTCCCTTCCTAC	CCGCTCCAGGTACAGATTATTGT
Mouse-Bnip3	TGAAGTGCAGTTCTACCCAGG	CCTGTCGCAGTTGGGTTC
Mouse-LC3	CACTGCTCTGTCTTGTGTAGGTTG	TCGTTGTGCCTTTATTAGTGCATC
Mouse-Fis1	AAAGATGGACTGGTAGGCATG	AGGATTTGGACTTGGAGACAG
Mouse-Mfn2	GGTGGTATGACCAATCCCAG	GCACATGAAGGTGGCTTTTT
Mouse-Drp1	TGACCACACCAGTTCCTCTG	TGCCTCAGATCGTCGTAGTG

Transparent methods

Animals

C57BLKS/J-Leprdb/Leprdb (Db/Db) male mice (3-weeks old) purchased from the Model Animal Research Center of Nanjing University. Male C57BL/6J mice (6-8 weeks old) were purchased from Vital River Laboratories (Beijing, China) and housed under 22±2°C and 55%±10% humidity with 12-hour light-dark cycle.

For the DIO mice model, eight mice were fed a low-fat diet (LFD), and the rest mice were fed high-fat-diet (HFD) until the weight difference was over 18-20% for six weeks (Figure S1A). We marked the mice fed an LFD and sterile water as the vehicle control group (LFD, n = 8). The HFD mice divided into four groups: control group (HFD, n = 8) fed an HFD and sterile water, and three treatment groups fed an HFD and ALLICIN solutions (Allicin-High, Allicin-Mid, Allicin-Low with 0.3%, 0.6%, 1% m/m ALLICIN solution for drinking, respectively, n = 8). The experiment lasted for another 13 weeks. ALLICIN solutions refreshed every 1-2 days. ALLICIN (98%, YZ-100384, Solarbio) purchased from Solarbio Life Science Biotechnology Co. Ltd. All experimental procedures conducted and the animals used according to the Guide for the Care and Use of Laboratory Animals published by the U.S. National Institute of Health and approved by the Animal Ethics Committee of China Agricultural University, Beijing.

Human subjects

The human adipocytes were obtained as previously described (Wu et al. 2016). Human embryonic brown adipose tissue was obtained from spontaneous abortions (11 weeks of gestation) at the Department of Gynecology and Obstetrics in Lu He hospital. Subcutaneous adipose tissues were dissected from the leg and back of the embryo. In parallel, adult subcutaneous fat tissues were obtained from a colon cancer patient in the Department of Surgery in Lu He Hospital. Fetal parents and patients were free of cardiovascular disease, endocrine diseases, metabolic disorders, and acute infection. Isolation of stem cells/primary adipocytes from adipose tissues of human embryo and adult subcutaneous fat was performed as described previously (Wu et al. 2016). Briefly, immediately after dissection, freshly resected fat depots were collected, minced, and digested using collagenase I (2 mg/mL in PBS with the addition of 3.5% BSA; Worthington Biochemical Corporation, Lakewood, NJ) and the stromal vascular fraction (SVF) was isolated. Floating adipocytes were separated from the SVF by centrifugation at 300× g for 3 min. The study complied with the Helsinki Declaration for investigation of human subjects. It received ethical approval from the competent Institutional

Brown differentiation of primary human adipocytes

After isolation, primary adipocytes were plated and grown in high-glucose Dulbecco's modified Eagle's medium (DMEM/H) supplemented with 20% (vol/vol) fetal bovine serum (FBS) (Sigma-Aldrich) and 1% penicillin-streptomycin. For adipocyte differentiation, cells were grown to reach 100% confluence and then exposed to adipogenic induction mixture in DMEM/H medium containing 0.5 mM isobutylmethylxanthine, 0.1 μM dexamethasone, 0.5 μM human insulin (Sigma-Aldrich, Dallas, TX), 2 nM T3, 30 μM indomethacin, 17 μM pantothenate, 33 μM biotin and 2% FBS for 6–7 days. Adipocyte differentiation medium was refreshed every 2 days in the entire experiments. To investigate the brown adipocyte activity, on the last day of differentiation, cells were stimulated with 50 μM Allicin for 24 hours. To measure the beiging ability of human white adipocytes, primary cells were stimulated with 50 μM Allicin for 7-10 days. Cells were collected for RNA extraction or western blot.

Glucose tolerance test and insulin tolerance test

GTT and ITT performed during the last week of the experiment. For GTT, mice fasted for 16h with free access to drinking water. Glucose (0.8 g/kg for Db/Db mice and 1.5 g/kg for HFD and LFD mice) was administered intraperitoneally, and blood glucose levels were measured with an Accu-Chek glucose monitor (ACCU-CHEK, Shanghai, China) at 0, 15, 30, 60, 90 and 120 min. For the insulin tolerance test (ITT), the mice fasted for 4 h (9:00 AM to 1:00 PM), and the mice were administered human insulin (0.7 U/kg

Humulin R; Novo Nordisk) by intraperitoneal injection. Blood glucose concentrations were determined from the tail vein with a blood glucose meter (ACCU-CHEK) at 0, 15, 30, 45, and 60 min after the insulin injection.

Cold-induced thermogenesis

For cold tolerance test, mice were placed in a cold chamber (4°C) for four h. We evaluated the cold-induced thermogenesis by measuring the rectal temperature with a temperature sensor (AT210, Zhongyidapeng, Shenzhen, China). Then we took infrared thermal imaging of the animals by a handheld infrared camera (FLIR T600) on a whiteboard.

Metabolic rate and physical activity

Oxygen consumption and physical activity were determined at the 12th week of the experiment with a TSE lab master (TSE Systems, Germany) (Liu et al. 2013). Mice were acclimated to the system for 20–24h, and then we measured oxygen consumption (VO_2 and VCO_2) over the next 24 h. The animals were maintained at 25°C in a 12-h light/dark cycle with free access to food and water. We measured the voluntary activity of each mouse using an optical beam technique (Opto-M3, Columbus Instruments, Columbus, OH, USA) over 24 h and expressed as 24 h average activity. The respiratory exchange ratio (RER) was then calculated (Livak and Schmittgen 2001).

Body composition measurements

The total fat and lean masses of mice after a 12-week treatment with either vehicle or ALLICIN were assessed with the Small Animal Body Composition Analysis and Imaging System (MesoQMR23-060H-I, Nuimag Corp., Shanghai, China), according to the manufacturer's instructions.

Positron emission-computed tomographic imaging

Specific method reference from Yuan et al. Briefly described as the mice were left unfed overnight and was lightly anesthetized with isoflurane followed by a tail vein injection of fluorodeoxyglucose ([18F]-FDG; 500 mCi). They were subjected to PET-CT analysis at 60min after radiotracer injection. Inveon Acquisition Workplace (IAW) software (Siemens Preclinical Solutions) was used for the scanning process. A 10-min CTX-ray for attenuation correction was scanned with a power of 80 kV and 500 mA and an exposure time of 1100ms before the PET scan. Ten-minute static PET scans were acquired, and images were reconstructed by ordered-subsets expectation maximization (OSEM) 3-dimensional algorithm followed by maximization/maximum a posteriori (MAP) or Fast MAP provided by IAW. The 3-dimensional regions of interest (ROIs)were drawn over the guided CT images, and the tracer uptake was measured with the IRW software (Siemens). Specific quantification of the [18F]-FDG uptake in each of the ROIs was calculated. The data for the accumulation of [18F]-FDG on micro-PET images were expressed as the standard uptake values, which were determined by dividing the relevant ROI concentration by the ratio of the injected activity to the bodyweight.

Histology and Oil-red-o staining

Tissues fixed with 4% paraformaldehyde were sectioned after embedment in paraffin. We prepared multiple sections for hematoxylin-eosin staining. We incubated cells grown on poly-L-lysine-pretreated coverslips (Sigma-Aldrich, St. Louis, MO, USA) in 5% goat serum for 1 h at room temperature after fixation with 1% formalin at room temperature for 1 h; To detect neutral lipid in liver, cells were stained with 0.2%(w/v) Oil-Red O (Sigma-Aldrich, St. Louis, MO,USA) for 10 min at room temperature after fixation with 4%PFA. All images were acquired with the BX51 system (Olympus, Tokyo, Japan).

Transmission electron microscopy

BAT sections were fixed with 2% v/v glutaraldehyde in 100mM phosphate buffer (pH 7.4) for 12 h at 4℃. Sections were then postfixed with 1% osmium tetroxide, dehydrated in ascending gradations of ethanol and embedded in fresh epoxy resin 618. Ultrathin sections(60–80nm) were cut and stained with lead citrate before being examined on a Hitachi H-7500 transmission electron microscope.

Mouse Brown adipocyte differentiation

The isolation method of mouse BAT primary cells referred to (Yuan et al. 2017). Primary cells were cultured in basal medium (containing 80% DMEM, 20% fetal bovine serum, and 1% penicillin and streptomycin) until the cells had reached more than 90% confluency. Then, cells were treated with a brown adipogenic induction cocktail (DMEM) containing 10% fetal bovine serum, 1% penicillin and streptomycin, 20 nM insulin, 1 mM dexamethasone, 0.5 mM isobutylmethylxanthine, 125 nM indomethacin, and 1 nM 3,3,5-triiodo-L-thyronine (T3) for the first two days. The medium was then replaced by the medium supplemented with only insulin and T3 every other day. The cells were treated with or without ALLICIN (50 µg/mL, SA8720, Solarbio) for six days during brown adipogenesis. BAT differentiation medium was used as the solvent, and 0.1 µg/mL, 1 µg/mL, 10 µg/mL, 50 µg/mL and 100 µg/mL solutions were used as the material for the *in vitro* tests. At day 6, fully differentiated adipocytes were used for the experiments.

Measurements of cellular respiration

BAT primary adipocytes were treated with and/or without Allicin (50 µg/mL) at day 6 of brown adipogenesis for 24h. We measured O_2 consumption of fully differentiated adipocytes at day 7 with an XF24-3 extracellular flux analyzer (Agilent Technologies, Santa Clara, CA, USA). Basal respiration was also assessed in untreated cells.

RNA isolation and real-time quantitative PCR

Total RNAs from tissues or cells were extracted with Trizol reagent (Thermo Fisher Scientific). We used equal amounts of RNA to synthesize cDNA with the transcript One-Step gDNA Removal and cDNA Synthesis SuperMix kit (AT311-03, TransGen Biotech, Beijing, China). The PCR reaction was run in triplicate for each sample using a Prism VIIA7 real-time PCR system (Thermo Fisher Scientific). Primer sequences are available upon request.

Western blot analysis

An equal amount of protein from cell lysate was loaded into each well of a 12%SDS-polyacrylamide gel after denaturation with SDS loading buffer. After electrophoresis, we transferred proteins to a PVDF membrane and incubated with blocking buffer (5% fat-free milk) for 1 h at room temperature. The following antibodies were added overnight: anti-UCP1 (Abcam, ab10983, 1:1000 diluted in 5% BSA, 0.0025% Tween-20 in 1× TBS solution), anti-Oxphos (Abcam, ab110413, 1:1000 dilution), anti-LC3 (CST, 4108, 1:1000 dilution), anti-sirt5 (santa cruz, sc-271635, 1:1000 dilution), Pan anti-succinyllysine antibody (PTM Biolabs, PTM-401, 1:1000 dilution), anti-β-actin (CST, #8457, 1:1000 dilution) and anti-β-tubulin (CST, #2146, 1:1000 dilution). These primary antibodies were incubated overnight in a 4°C refrigerator. The membrane was incubated with horseradish peroxidase-conjugated secondary antibodies for 1 h at room temperature. All signals were visualized and analyzed by Clinx Chemi Capture software (Clinx, Shanghai, China).

Immunofluorescence staining

We stained differentiated cells with anti-human UCP1, followed by an Alexa 488-conjugated secondary antibody (Invitrogen, Carlsbad, CA, USA), BODIPY (Thermo Fischer Scientific, Waltham, MA, USA) and DAPI (Leagene, Beijing, China), complying with manufacturers' the procedure. Brown adipocytes were positive for both UCP1 and BODIPY. We stained negative controls with the omission of a primary antibody. Images were taken by Zeiss laser scanning confocal microscopy (LSM780, Oberkochen, Germany).

Immunoprecipitation studies

BAT or brown adipocytes were lysis in RIPA buffer. UCP1 protein was immunoprecipitated using anti UCP1 antibody (Rabbit monoclonal; Abcam) and then detected using a pan anti-succinyllysine antibody (PTM Biolabsd).

PGC1a/Sirt1 acetylation assay

Brown adipocytes were transfected with the plasmids of His-PGC1a (2 μg), SIRT1 (0.5μg), and p300 (0.5 μg). Twenty-four hours after transfection, the cells were incubated with or without Allicin, and then the cell lysates were collected with IP buffer [50mM4-(2-hydroxyethyl)1-piperazineethanesulfonic acid (HEPES;pH7.9),150mMNaCl, 10% glycerol,1 mM EGTA, 1% Triton X-100, 0.5% NP-40, 1 mM trichostatin A (TSA), and protease inhibitor cocktail (Roche)], followed by incubation with anti-PGC1a antibody (H300; Santa Cruz Biotechnology) and/or anti-SIRT1 (Cell Signaling Technology, Danvers, MA, USA) overnight at 4°C. Immunoprecipitates were blotted with anti-acetyl-lysine (EMS–Millipore) and Pan anti-succinyllysine antibody (PTM Biolabs, PTM-401, Hangzhou, China) antibodies.

Measurement of Mitochondrial DNA Copy Number

Total DNA (genomic and mitochondrial DNA) was extracted from the differentiated human primary BAT cells using a QIA amp DNA Mini kit (Qiagen, Venlo, Netherlands) according to the manufacturer's instructions. DNA concentrations were assessed using a Nanodrop 2000 (Thermo Scientific, Wilmington, DE, USA). The mitochondrial DNA (mtDNA) copy number relative to genomic DNA content was quantitatively analyzed using an ABI Prism VIIA7 real-time PCR (Applied Biosystems, Waltham, MA, USA). Primer sequences for COXII and β globin were as follows: COXII: forward GCCGACTAAATCAAGCAACA, reverse CAATGGGCATAAAGCTATGG, β globin: forward GAAGCGATTCTAGGGAGCAG, reverse GGAGCAGCGATTCTGAGTAG.

Statistical analysis

Data are expressed as means ± SE. Statistics were performed using a repeated measure two-way analysis of variance (ANOVA), the one-way ANOVA test, analysis of covariance (ANCOVA) or Student's t-test. Significant differences were considered when $P < 0.05$.

References for supplemental information

Livak, K. J.; Schmittgen, T. D. (2001): Analysis of relative gene expression data using real-time quantitative PCR and the 2(-Delta Delta C(T)) Method. In *Methods (San Diego, Calif.)* 25 (4), pp. 402–408. DOI: 10.1006/meth.2001.1262.

Liu, Xiaomeng; Zheng, Zongji; Zhu, Xiaoming; Meng, Minghui; Li, Lan; Shen, Yanyan et al. (2013): Brown adipose tissue transplantation improves whole-body energy metabolism. In Cell research 23 (6), pp. 851–854. DOI: 10.1038/cr.2013.64.

Yuan, Xiaoxue; Wei, Gang; You, Yilin; Huang, Yuanyuan; Lee, Hyuek Jong; Dong, Meng et al. (2017): Rutin ameliorates obesity through brown fat activation. In FASEB journal: official publication of the Federation of American Societies for Experimental Biology 31 (1), pp. 333–345. DOI: 10.1096/fj.201600459RR.

Wu, Nan-Nan; Zhang, Chuan-Hai; Lee, Hyuek-Jong; Ma, Yan; Wang, Xin; Ma, Xiao-Juan et al. (2016): Brown adipogenic potential of brown adipocytes and peri-renal adipocytes from human embryo. In *Scientific reports* 6, p. 39193. DOI: 10.1038/srep39193.